Observations on Palaeogeographical Evolution of Akrotiri Salt Lake, Lemesos, Cyprus

Miltiadis Polidorou, Niki Evelpidou, Theodora Tsourou, Hara Drinia, Ferréol Salomon, Lucy Blue

geosciences

MDPI

Article

Observations on Palaeogeographical Evolution of Akrotiri Salt Lake, Lemesos, Cyprus

Miltiadis Polidorou [1,*], Niki Evelpidou [1], Theodora Tsourou [1], Hara Drinia [1], Ferréol Salomon [2] and Lucy Blue [3]

[1] Faculty of Geology and Geoenvironment, National and Kapodistrian University of Athens, 15774 Athens, Greece; evelpidou@geol.uoa.gr (N.E.); ttsourou@geol.uoa.gr (T.T.); cntrinia@geol.uoa.gr (H.D.)
[2] Laboratoire Image Ville Environnement (UMR-7362), Centre National de la Recherche Scientifique (CNRS), Université de Strasbourg, 3 rue de l'Argonne, 67000 Strasbourg, France; ferreol.salomon@live-cnrs.unistra.fr
[3] Centre for Maritime Archaeology, School of Humanities, University of Southampton, Avenue Campus, Highfield, Southampton SO17 1BJ, UK; lkb@soton.ac.uk
* Correspondence: mpolidorou@geol.uoa.gr

Abstract: Akrotiri Salt Lake is located 5 km west of the city of Lemesos in the southernmost part of the island of Cyprus. The evolution of the Akrotiri Salt Lake is of great scientific interest, occurring during the Holocene when eustatic and isostatic movements combined with local active tectonics and climate change developed a unique geomorphological environment. The Salt Lake today is a closed lagoon, which is depicted in Venetian maps as being connected to the sea, provides evidence of the geological setting and landscape evolution of the area. In this study, for the first time, we investigated the development of the Akrotiri Salt Lake through a series of three cores which penetrated the Holocene sediment sequence. Sedimentological and micropaleontological analyses, as well as geochronological studies were performed on the deposited sediments, identifying the complexity of the evolution of the Salt Lake and the progressive change of the area from a maritime space to an open bay and finally to a closed salt lake.

Keywords: palaeogeography; salt lake; landscape evolution; Holocene; coastal geomorphology; micropalaeontology; palaeoenvironment

Citation: Polidorou, M.; Evelpidou, N.; Tsourou, T.; Drinia, H.; Salomon, F.; Blue, L. Observations on Palaeogeographical Evolution of Akrotiri Salt Lake, Lemesos, Cyprus. *Geosciences* **2021**, *11*, 321. https://doi.org/10.3390/geosciences11080321

Academic Editors: Maša Surić, Lara Wacha and Jesus Martinez-Frias

Received: 24 May 2021
Accepted: 12 July 2021
Published: 30 July 2021

1. Introduction

Coastal lagoons and associated salt marshes are dynamic environments, which change under the impact of local, regional and global actions such as waves, tides, fluvial influence, climatological factors, coastal and subaerial erosion and sea level fluctuations [1]. Coastal lagoons are very common in Mediterranean coast-lines. They are inland waterbodies, usually developing parallel to the coast and separated from the open sea by a sandy barrier [2–4]. They can be permanently open or intermittently closed off [5]. Typically, one or more restricted inlets ensure their continuous or intermittent connection to the open sea. Water depth varies from a few centimeters up to a few meters [6].

The evolution of a coastal lagoon from an open to a semienclosed environment is commonly recorded in Holocene buried lagoonal successions [7,8]. The gradual development of sandy barriers favors the progressive isolation of the brackish water body [4].

Sedimentological, palaeontological, geochemical and mineralogical studies at lagoonal successions provide information regarding depositional environments, elemental fluxes, palaeoclimate, sea level fluctuation, tsunamigenic phenomena and tectonic activity [9–13]. Lagoonal geochemical profiles, such as relative changes and altering trends of elemental concentration, can provide information about palaeoenvironmental changes [8,14,15]. Concerning micropalaeontological analysis, ostracods and benthic foraminifera are commonly used to provide evidence on changes of the depositional environment. Ostracods are small,

bivalved crustaceans inhabiting most aquatic environments and are sensitive to environmental changes [16,17]. They are extensively used in interpreting palaeoenvironmental conditions, especially in the fragile coastal marine ecosystems where sea level changes and climatic oscillations are recorded [18–20]. Benthic foraminifera are unicellular organisms that are abundantly present in the marine realm. These benthic organisms are widely used as tools for the reconstruction of palaeoenvironments, as they generally inhabit relatively narrow ranges of environmental conditions. They are especially suitable for monitoring rapid environmental changes because many species are opportunistic, rapidly responding to environmental change [21–26].

Palaeoenvironmental reconstructions may significantly improve our understanding of past human interactions with the environment and the impact of relative sea-level changes on the coastal environment [10,13,27–29]. Furthermore, paleoenvironments formed during the Late Quaternary provide significant information in estimating the response of present-day coastal areas to future sea level and climate changes [30–32].

The purpose of this study was the palaeogeographic reconstruction of the Akrotiri Salt Lake through a multiproxy approach which includes sedimentological, micropalaeontological, geochemical and mineralogical analyses of the retrieved sediment cores. This is the first time that such a combined study has taken place in this significant area and aims to provide valuable data regarding the development of such types of coastal environments in the context of relative sea level change, neotectonic movements, geomorphological evolution and climatological change since the beginning of the Holocene in the eastern Mediterranean.

2. Study Area

The Akrotiri peninsula is located 5 km west of Lemesos city and is the southernmost part of the island of Cyprus (Figure 1). It consists of Quaternary sediments which have been unconformably deposited on Miocene chalks and marls of the Pachna formation [33]. The Quaternary sediments are composed of fluvial, marine, deltaic, aeolian and lagoonal deposits [34] (Figure 2). In the central part of the peninsula the Akrotiri Salt Lake dominates the topography, covering an area of approximately 20 km^2. Today, the maximum depth of the Salt Lake reaches 2.8 m below mean sea level during the winter period. On the western part of the peninsula an extensive tombolo has developed, which consists of deltaic and aeolian deposits. To the east of the Salt Lake, there are series of sand dunes and sandy beach bars. The northern area is covered by Quaternary alluvial fans, which were formed by the discharged material of Kouris River, the largest river in Cyprus. In the southern region of the Peninsula, uplifted marine terraces are overlapped by sandy layers of aeolian origin [34] (Figure 2).

The development of the peninsula started with the deposition of calcareous marls in the Episkopi grabben during the Miocene, which resulted in the Akrotiri high topography on the south in the form of an isolated island [35]. The marine strait between the Akrotiri Island and the mainland eventually closed during the Quaternary, and several geomorphic features were developed.

The Quaternary tectonic setting of the area [36] is indicating a gradual uplift of the southwest area of Akrotiri peninsula which was driven by a left lateral strike slip fault with vertical components (Figure 2).

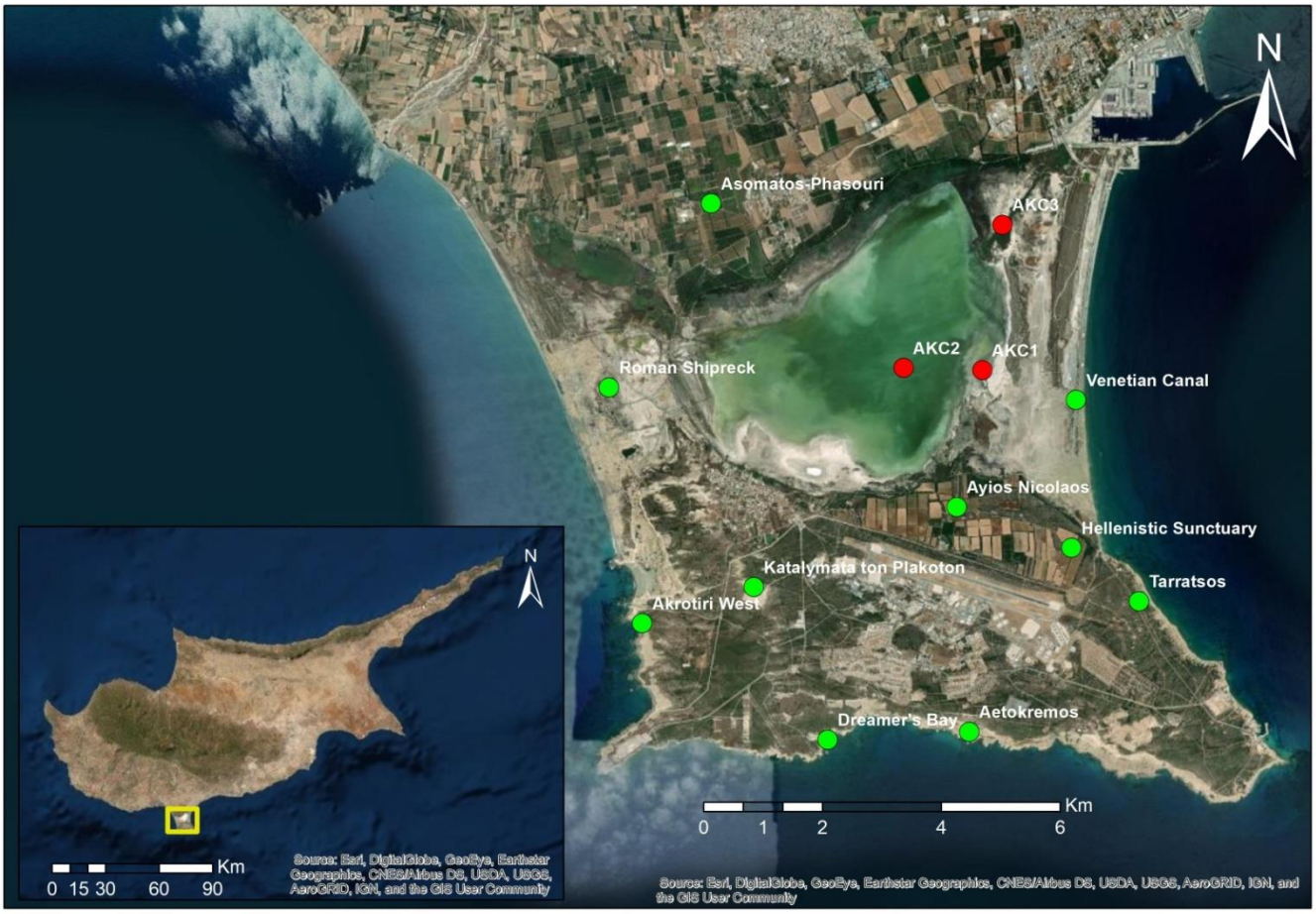

Figure 1. Study area of the Akrotiri Peninsula and archeological sites (green dots) and evidence of human occupation dated from the Epipaleolithic period (12,000 BP) until the present day (Satellite photography of the study area. Red dots represent the locations of the cores (Source: Esri, DigitalGlobe, GeoEye, Earthstar Geographics, CNES/Airbus DS, USDA, USGS, AeroGRID, IGN, and the GIS User Community).

The Akrotiri Peninsula has a plethora of archaeological sites, and evidence of human occupation is dated from the Epipaleolithic period (12,000 BP) until the present day (Figure 1). It is considered as the most important archaeological area in Cyprus. The Akrotiri Peninsula contains the earliest evidence of human colonization on Cyprus at ~12,000 BP at the Aetokremnos site, which is located at the center of the southern coast line of the study area [37–41]. During the Bronze Age (2500–1050 BC) there were numerous sites located along Kouris River and around the Salt Lake. The first evidence of substantial activity occurring in the area dates back to the Late Hellenistic- Early Roman Period (1st century BC–1st century AD), which appears to the southern end of the peninsula and continues through the Late Roman to Early Byzantine period (3rd century AD–4th century AD) with a number of settlements [42,43] and Dreamer's Bay harbor [44]. Evidence of Frankish and Venetian Period (1191–1571 AD) also appears in the area, such as the Venetian canal at the east of the Salt Lake. Maps and historical documents from that period (Venetian) depict the study area and have been used for the interpretation of the paleoenvironmental evolution of the area.

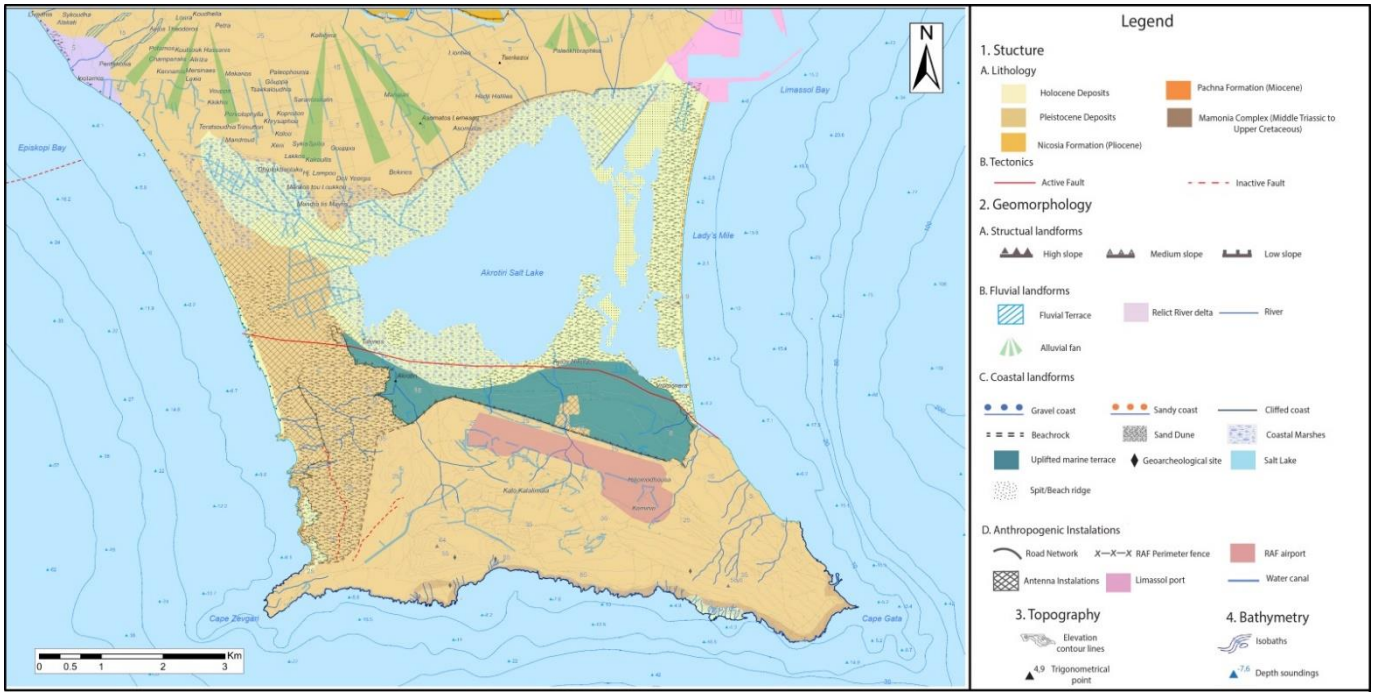

Figure 2. Geomorphological map of the Akrotiri Peninsula [34].

3. Materials and Methods

Geomorphological mapping and a field survey of the coastal area of Akrotiri Peninsula was conducted with the use of topographic maps at a scale of 1:5000. Orthomaps acquired by the Cyprus Land and Survey Department, and Quickbird satellite images (https://portal.dls.moi.gov.cy/, accessed on 20 May 2020) were introduced and analyzed in the GIS environment. Historical maps relative to the area dated from the fifteenth century AD, and historical bibliographic literature were also taken into account for the geomorphological analysis of the study area.

For the evaluation of the palaeogeographical evolution of the studied area, three shallow cores (AKC1, AKC2 and AKC3) were retrieved from the eastern side of the Akrotiri Salt Lake. The cores were extracted using an Atlas Copco Cobra 32T vibracorer, (Stockholm, Sweden) with a 5.5 cm diameter plastic PVC tube in a metal tube housing and a titanium drilling head. The deepest core, AKC3, reached 3.4 m in depth, AKC1 2.6 m and AKC2 1.95 m. The site water depth at the time of AKC2 coring was approximately 0.7 m. The cores were sealed and transported at the laboratory of Mechanical Geology and Industrial Minerals of the Cyprus Geological Survey Department. The positions of the cores were measured with a Spectra SP80 differential GPS/GNSS system, (California, USA) receiver with vertical and horizontal accuracies of less than 2 cm.

The stratigraphic analysis of the cores was accomplished by studying sedimentary facies through visual inspection of the sediments. Detailed grain size analyses were performed on the collected core sediment samples, which included grain size analyses, hydrometric analyses and sieving analyses. For the determination of grain size, 43 samples were analyzed and classified based on Folk's [45] nomenclature.

Downcore relative elemental composition of sediment cores were analyzed using an Olympus Vanta handheld XRF scanner equipped with the Olympus, (Tokyo, Japan) "Geochem" Suite. Analysis of the elemental composition was performed using an X-ray source with the voltage set to 8–40 kV, which enabled measurements of major and minor elements (Mg; Al; Si; P; S; K; Rb; Ca; Sr; Ti; V; Cr; Mn; Fe; Co; Ni; Cu; Zn; As; Se; Y; Zr; Nb; Mo; Ag; Cd; Sn; Sb; W; Au; Hg; Pb; Bi; Th and U) [46] (Tables A1 and A2). The acquired XRF data were reported as elemental ratios [15,47–49] (Table A3). For the purposes of this study the elemental ratios of Sr/Ca and Ti/Ca were selected. Sr is an alkaline earth

metal fixed by calcifying organisms at the same time as Ca. Hence Sr is a marker for biogenic origin. As Ca can be supplied from terrigenous sources (e.g., feldspars and clays) covariation of Ca and Sr suggests Ca was mainly be sourced from biogenic $CaCO_3$. Sr/Ca is used as a proxy for aragonite, thus enhanced Sr may indicate the presence of high-Sr aragonite, which requires a shallow-water source [50]. Ti is a conservative element that generally varies directly with the coarse-grained terrigenous fraction. It is a common constituent of rocks, such as gneisses or schists, and it primarily indicates a terrigenous continental source. Moreover, Ti occurs in all minerals commonly associated with sand and silt fractions. Ti is widely used to record terrigenous sediment delivery. It commonly covaries with Fe but is arguably a better proxy for terrigenous sediment delivery than Fe, as it is redox-insensitive [51,52]. Ti/Ca records the relative variation of terrigenous input and marine carbonate [53,54]. It has been used to record changes from fluvial to marine deposits, for example, in incised-valley-fill sediments [55].

A total of 73 samples from the three cores were selected for micropalaeontological analysis, 26 samples from AKC1, 17 samples from AKC2 and 30 samples from AKC3. A fraction of 10 gr (dry weight) from each sample was treated with H_2O_2, wet sieved and dried. Ostracods and benthic foraminifers were collected from the fraction >125 μm. All ostracods were collected from each sample (Tables A4–A8). When the specimen abundance was too high, aliquots were examined in order to collect at least 200 valves per sample. The identification of ostracod species was based on several publications [20,56–61]. Due to their low abundance and low diversity, the benthic foraminifers were not statistically processed. Where possible, an average of 200 foraminifer specimens were randomly picked from each fraction >0.125 mm. In the case of a very low density of specimens (usually in sandy sediments), the entire dried residue was microscopically examined (Table A9). Ecological information, especially on depth, hydrodynamism, salinity and substrates, was extracted from the abundant available literature dealing with benthic foraminifers [62–65].

Geochronological studies with AMS radiocarbon dating were applied on seven samples (mollusk shells) which were extracted from the cores by the CEntro di DAtazione e Diagnostica (CEDAD) in Lecce, Italy. Radiocarbon ages were calibrated through the online software Calib 7.10 [66] using the INTCAL13 atmospheric data set for terrestrial samples and the MARINE13 curve for marine samples [67] with a DR value of -52 ± 50 estimated for the eastern Mediterranean [68].

4. Results

All the cores were studied regarding their stratigraphy and grain size analysis, hydrometric and sieving analyses. Sedimentological statistical parameters such as mean, sorting, skewness, and kurtosis were calculated using Gradistat V.4 software and they appear in Table 1 [69].

4.1. AKC1

Sediment core AKC1 was subdivided into five lithological units. On the lowermost lithological unit LU1a, homogenous whitish-grey sediments with the presence of small, rounded gravels were recognized in the interval between 260 cm and 230 cm. The sediment was predominantly constituted of high percentages of clay and fine sand sized particles (~63%). The lowermost part of core AKC1 was characterized by medium Sr/Ca and Ti/Ca ratios (Figure 3). Ostracod assemblages (Figure 4) were characterized by the abundance of *Cyprideis torosa*, an euryhaline species, abundant or dominant in assemblages for all the transitional environments, especially in shallow lagoons (<30 m depth) and estuaries when salinity ranges between 2–17‰ [60,70,71]. *Cyprideis torosa* was accompanied by the polyhaline–euhaline shallow water species *Basslerites berchoni* [61,72], the marine species *Xestoleberis communis* and *Aurila woodwardia,* which are mainly epiphytal, tolerating salinity fluctuations, and occur also in brackish environments [58,73–75], and other shallow littoral marine taxa such as *Loxoconcha* species (mainly with the mostly epiphytal species

L. affinis; [58,75]) and *Phlyctenophora* sp. Benthic foraminiferal fauna was oligospecific, mainly dominated by Miliolidae (~30%) and *Ammonia tepida* (~25%).

Table 1. Sedimentological statistics, mean, sorting, skewness, and kurtosis calculated using Gradistat V.4 software [69].

Core ID	Sample No.	Depth (cm)	Mean	Sorting	Skewness	Kurtosis
AKC1	74	0–34	Fine Sand	Moderately Well Sorted	Symmetrical	Platykurtic
AKC1	75	34–42	Fine Sand	Moderately Well Sorted	Fine Skewed	Platykurtic
AKC1	76	42–60	Fine Sand	Moderately Well Sorted	Fine Skewed	Platykurtic
AKC1	77	60–94	Fine Sand	Moderately Sorted	Very Coarse Skewed	Leptokurtic
AKC1	78	94–105	Fine Sand	Moderately Sorted	Very Coarse Skewed	Mesokurtic
AKC1	79	105–145	Fine Sand	Moderately Well Sorted	Coarse Skewed	Platykurtic
AKC1	80	145–172	Fine Sand	Moderately Well Sorted	Fine Skewed	Platykurtic
AKC1	81	172–189	Fine Sand	Moderately Well Sorted	Fine Skewed	Platykurtic
AKC1	82	189–198	Fine Sand	Moderately Sorted	Coarse Skewed	Platykurtic
AKC1	83	198–227	Fine Sand	Moderately Well Sorted	Coarse Skewed	Platykurtic
AKC1	84	227–231	Fine Sand	Moderately Well Sorted	Fine Skewed	Mesokurtic
AKC1	85	231–237	Fine Sand	Poorly Sorted	Very Coarse Skewed	Leptokurtic
AKC1	86	237–273	Fine Sand	Poorly Sorted	Very Coarse Skewed	Leptokurtic
AKC2	87	0–3	Fine Sand	Well Sorted	Fine Skewed	Leptokurtic
AKC2	88	3–17	Fine Sand	Moderately Well Sorted	Fine Skewed	Platykurtic
AKC2	89	17–27	Fine Sand	Poorly Sorted	Coarse Skewed	Very Leptokurtic
AKC2	90	27–39	Fine Sand	Moderately Sorted	Coarse Skewed	Mesokurtic
AKC2	91	39–49	Medium Sand	Poorly Sorted	Coarse Skewed	Platykurtic
AKC2	92	49–55	Medium Sand	Poorly Sorted	Coarse Skewed	Mesokurtic
AKC2	93	55–63	Medium Sand	Poorly Sorted	Coarse Skewed	Leptokurtic
AKC2	94	63–73	Fine Sand	Poorly Sorted	Coarse Skewed	Leptokurtic
AKC2	95	73–90	Medium Sand	Poorly Sorted	Coarse Skewed	Mesokurtic
AKC2	96	90–99	Medium Sand	Poorly Sorted	Coarse Skewed	Leptokurtic
AKC2	97	99–130	Medium Sand	Poorly Sorted	Coarse Skewed	Leptokurtic
AKC2	98	130–140	Medium Sand	Poorly Sorted	Coarse Skewed	Mesokurtic
AKC2	99	140–150	Medium Sand	Moderately Sorted	Coarse Skewed	Leptokurtic
AKC3	100	0–18	Fine Sand	Moderately Sorted	Coarse Skewed	Mesokurtic
AKC3	101	18–52	Fine Sand	Moderately Sorted	Coarse Skewed	Mesokurtic
AKC3	102	52–60	Fine Sand	Moderately Well Sorted	Symmetrical	Platykurtic
AKC3	103	60–83	Fine Sand	Moderately Well Sorted	Coarse Skewed	Platykurtic
AKC3	104	83–93	Fine Sand	Moderately Sorted	Coarse Skewed	Mesokurtic
AKC3	105	93–105	Fine Sand	Moderately Sorted	Coarse Skewed	Platykurtic
AKC3	106	105–116	Fine Sand	Moderately Sorted	Coarse Skewed	Mesokurtic
AKC3	107	116–144	Fine Sand	Moderately Well Sorted	Coarse Skewed	Platykurtic
AKC3	108	144–153	Fine Sand	Moderately Sorted	Coarse Skewed	Mesokurtic
AKC3	109	165–172	Fine Sand	Moderately Sorted	Coarse Skewed	Platykurtic
AKC3	110	197–199	Fine Sand	Moderately Sorted	Coarse Skewed	Mesokurtic
AKC3	111	199–220	Fine Sand	Moderately Well Sorted	Coarse Skewed	Platykurtic
AKC3	112	220–240	Fine Sand	Moderately Sorted	Coarse Skewed	Mesokurtic
AKC3	113	240–258	Fine Sand	Moderately Sorted	Coarse Skewed	Mesokurtic
AKC3	114	258–280	Fine Sand	Moderately Sorted	Coarse Skewed	Mesokurtic
AKC3	115	280–285	Fine Sand	Poorly Sorted	Very Coarse Skewed	Leptokurtic
AKC3	116	285–294	Fine Sand	Moderately Sorted	Coarse Skewed	Leptokurtic
AKC3	117	294–330	Fine Sand	Moderately Well Sorted	Symmetrical	Platykurtic
AKC3	118	330–338	Fine Sand	Moderately Sorted	Coarse Skewed	Platykurtic

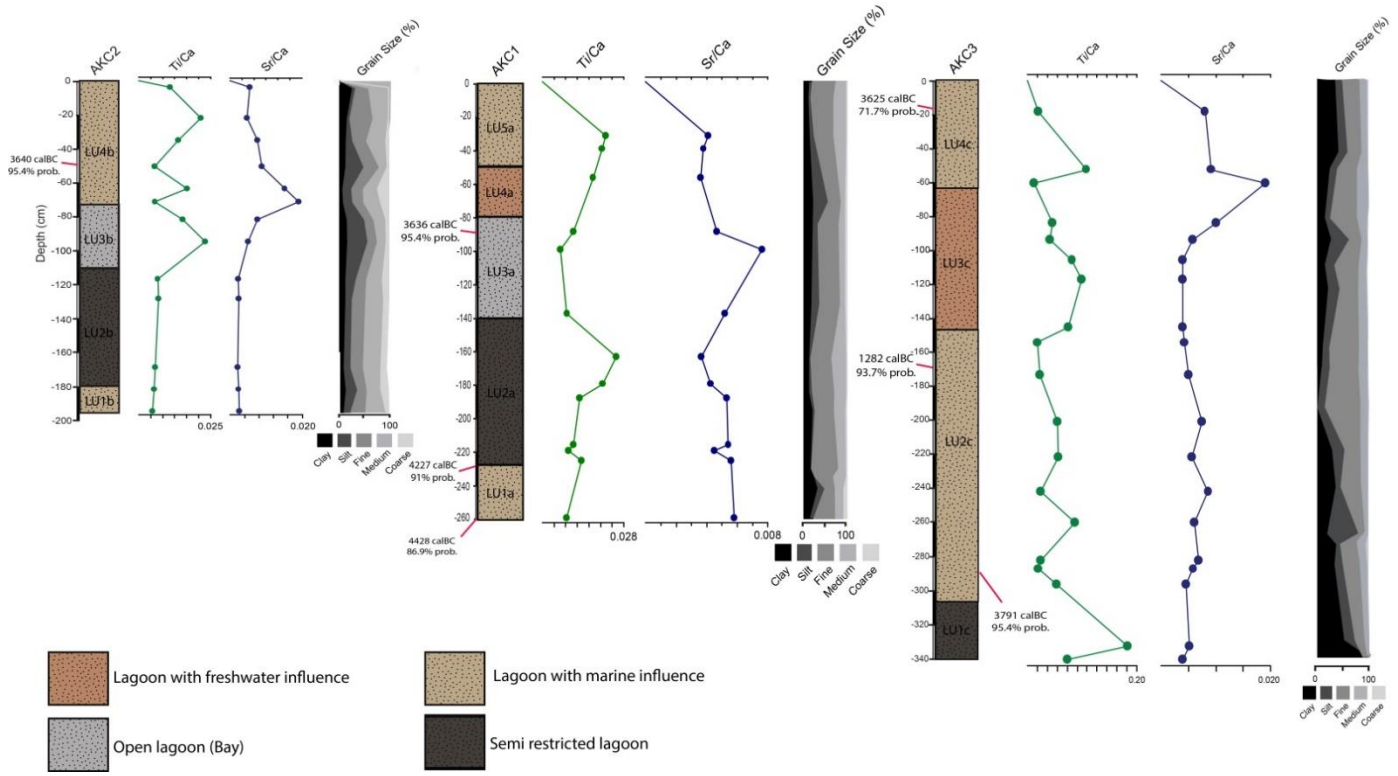

Figure 3. XRF data, grain size analysis and palaeoenvironmental interpretation of the cores.

Sediments of the overlying unit LU2a in core AKC1 (between 230 and 140 cm) appeared homogenous grey with the presence of fossil mollusk fragments and *Posidonia* fibers. This unit was characterized by a coarser grain size with high percentages of fine and medium sand sized particles (~79%). The acquired XRF data indicated an increase in Ti/Ca and a decrease in Sr/Ca ratios (Figure 3). Ostracod analysis (Figure 4) revealed low ostracod abundance and mixed assemblages, mainly with *C. torosa*, *X. communis*, *A. woodwardii*, *Phlyctenophora* sp., *L. affinis* and other shallow littoral marine taxa (e.g., [57,75]) such as species of *Semicytherura*, *Pontocythere* and *Urocythereis*. sp. Present in the samples were other open marine taxa (e.g., [57]) such as species of *Hiltermannicythere*, *Carinocythereis* and *Cytherella.* Benthic foraminiferal assemblages remained rather stable with the high presence of Miliolidae and *A. tepida*. At the level between 220 and 225 cm, *Nubecularia lucifuga* was present, indicating the existence of a sheltered bay. Seagrass (*Posidonia*) probably provided a substrate for attached forms.

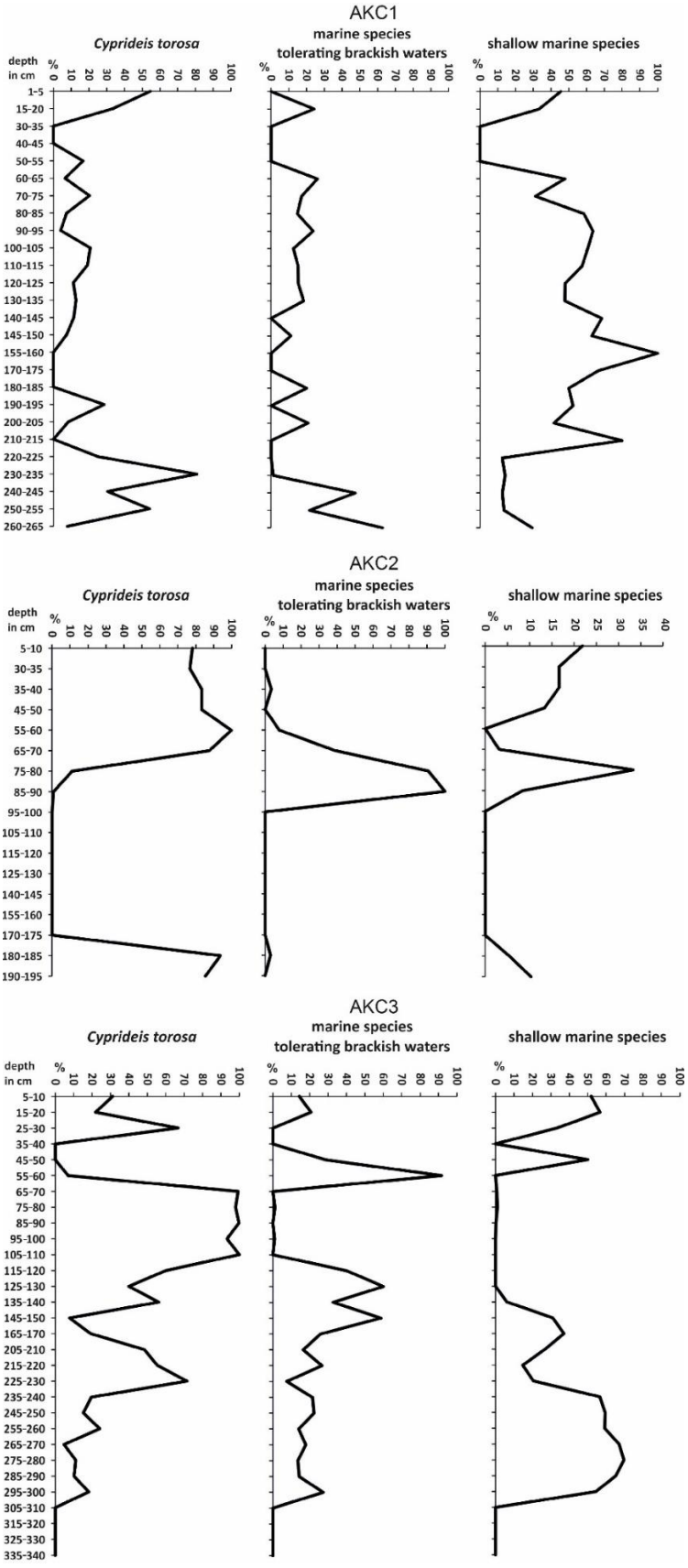

Figure 4. Distribution of ostracod assemblages along the cores. Marine species tolerating brackish waters: *B. berchoni, X. communis*, *A. woodwardii.* Shallow marine species: species of the genera *Loxoconcha*, *Phlyctenophora*, *Xestoleberis*, *Semicytherura*, *Pontocythere, Leptocythere* and *Urocythereis*. sp.

The third lithological unit, LU3a, was recognized in the core interval between 140 and 80 cm. Sediments in this unit were gray with a slightly finer grain size. Clay, silt and fine sand sized particles predominated (~85%). Some fossil mollusk fragments, and small rounded gravels were also observed. The obtained XRF data showed decreased values of Ti/Ca ratios (lower value in this core) and a significant increase of Sr/Ca ratios (higher value in this core) (Figure 3). Micropaleontological analysis revealed much richer ostracod faunas, mainly with *Loxoconcha* species, *C. torosa*, *Phlyctenophora* sp. and *X. communis*. The abundance of *Ammonia tepida* is in complete agreement with the lithological data and the ostracod fauna (Figure 4), further reinforcing the impression of a restricted marine environment.

Sediments of the lithological unit LU4a in core AKC1 between 80 and 50 cm were distinguished by their grey-greenish color and coarser grain size. LU4a was characterized by higher percentages of fine and medium sand sized particles (~76%). The Ti/Ca ratio increased and Sr/Ca ratio showed a decreased trend (Figure 3). Ostracods analysis revealed the presence of freshwater taxa [71] *Heterocypris salina* and *Limnocythere* sp. at the upper part of this unit.

Sediments of the topmost unit, LU5a, in the core AKC1 between 50 and 0 cm, appeared with a brown-grey color and a slightly coarser grain size. Fine and medium sand sized particles predominated, with percentages up to 82%. The Ti/Ca and Sr/Ca ratios showed increased values (Figure 3). Ostracod and benthic foraminiferal assemblages were very poor at the upper part of the sediment core, consisting mainly of shallow marine taxa (mainly *Ammonia* sp., *Cibicides* sp. and *Phlyctenophora* sp. and *Urocythereis* sp. respectively).

4.2. AKC2

Sediment core AKC2 was subdivided into four lithological units (Figure 3). The lowermost lithological unit, LU1b, was identified at the interval between 195 cm and 180 cm. Whitish-grey sediments with the presence of small angular gravel were identified. They were predominantly constituted of fine and medium sand sized particles (~74%). The lowermost part of core AKC2 was characterized by low Sr/Ca and Ti/Ca ratios (Figure 3). Ostracod assemblages of this unit were characterized by the dominance of *C. torosa* (Figure 4).

Sediments of the overlying unit LU2b in core AKC2 between 180 and 110 cm, appeared grey, with the presence of angular and square gravels. This unit was characterized by a coarser grain size with high percentages of fine and medium sand sized particles (~60%) and significant percentages of coarse sand sized particles (~15%). The acquired XRF data indicated stable values of Ti/Ca and Sr/Ca ratios (Figure 3). The interval between 180 and 110 cm was barren of microfossils.

The third lithological unit, LU3b, was recognized in the core interval between 110 and 75 cm. Sediments in this unit were whitish-gray with a significantly finer grain size. Clay and silt sized particles predominated with percentages up to ~55% (Figure 3). The obtained XRF data showed a rapid increase of Ti/Ca ratios (highest value in this core) followed by a rapid decrease and a steady increase of Sr/Ca ratios. Ostracod assemblages at this interval consisted mainly of *X. communis* and *A. woodwardii* (Figure 4).

Sediments of the topmost unit LU4b in core AKC3 between 75 and 0 cm), appeared with a grey to light-gray color and with a coarser grain size. Fine and medium sand sized particles appeared with percentages up to 70%. Clay and silt sized particles also appeared with a percentage of 47% at the depth of 39–27 cm. The Ti/Ca ratios values increased between 75 and 60 cm, which was followed by a decrease of the values between 60 cm and 50 cm, then an increase of the values between 50 cm and 20 cm, followed by a steady decrease up to the surface of the core. Sr/Ca ratios increased (higher value in this core) followed by a slow decrease up to the surface of the core (Figure 3). Ostracod assemblage was characterized by the dominance of *C. torosa* (Figure 4). The benthic foraminifer assemblage was characterized by *Peneroplis planatus* and *P. pertusus*, together with *Quinqueloculina* sp. and *Ammonia beccari*.

4.3. AKC3

The sediment core AKC3 was subdivided into four lithological units (Figure 3). The lowermost lithological unit LU1c was identified at the interval between 340 cm and 305 cm. Reddish- dark brown sediments were identified. They were predominantly constituted of silt and clay sized particles (~77%). The lowermost part of core AKC3 was characterized by increasing Ti/Ca ratios at 332 cm and followed by a slow decrease. Sr/Ca ratios were low and stable (Figure 3). Unit LU1c was barren of microfossils.

Sediments of the unit LU2c in core AKC3 between 305 and 145 cm) appeared greyish-brown with the presence of mollusk fragments and some small angular gravels on the 294–280 cm horizon. This unit was characterized by a slightly coarser grain size with percentages of fine sand of ~35% and clay and silt sized particles of ~45%. The acquired XRF data indicated stable values in Ti/Ca and Sr/Ca ratios with the exception of the Ti/Ca ratio peak at 260 cm (Figure 3). Ostracod assemblages (Figure 4) were composed mainly of *C. torosa*, *Phlyctenophora* sp., *A. woodwardii* and *Loxoconcha* spp.

The third lithological unit, LU3c, was recognized at the core interval between 145 and 65 cm (Figure 3). Sediments in this unit were reddish-brown with slightly finer grain size. Clay and silt sized particles appeared with percentages up to ~50%, with fine sand sized particles up to 40% (Figure 3). The obtained XRF data showed an increase of Ti/Ca ratios followed by a decrease and a steady increase of Sr/Ca ratios peaking to their highest value for this core at the upper part of this lithological unit (Figure 3). The ostracod faunas were characterized by the high abundance of *C. torosa*, forming, especially between the interval 105–65 cm, nearly monospecific assemblages (Figure 4), while the presence of the species *H. salina* at level 95–100 cm indicated freshwater input.

Sediments of the topmost unit LU4c in core AKC3 between 65 and 0 cm appeared with a brownish-grey color and a slightly finer grain size (Figure 3). Fine sand sized particles appeared with percentages up to 30%. Clay and silt sized particles appeared with percentages of 54%. The Ti/Ca ratios showed an increase at 50 cm (highest values for this core) followed by a decrease. Sr/Ca ratios showed a significant decrease up to the surface of the core (Figure 3). Ostracod assemblages (Figure 4) presented similar compositions to those of unit LU2c at the lower part of AKC3.

4.4. Geochronology

In total, seven samples (mollusk shells) from all the cores were processed for AMS radiocarbon chronology (Table 2). From core AKC1, three samples were selected (LTL19232A, LTL19233A, LTL19234A) at depths of −90 cm, −230 cm and −260 cm. The ages provided from a geochronological analysis and calibrations were 3510–3110 cal BC (95.4%, 2 sigma), 4072–3727 cal BC (95.4%, 2 sigma) and 4328–4017 cal BC (95.4%, 2 sigma) for the above-mentioned depths.

Table 2. Age determination results (at 2-sigma) of the selected samples. Age calibrated using MARINE13 curve for marine samples [67] with a DR value of −52 ± 50 estimated for the eastern Mediterranean [68].

Core ID	Sample No.	Type of Sample	Depth (cm)	Age (Years BC)	Calibrated Age at 2-Sigma (Years BC)
AKC1	LTL19232A	Mollusk Shells	−90	4902 ± 45	3510–3110 cal BC
AKC1	LTL19233A	Mollusk Shells	−230	5434 ± 45	4072–3727 cal BC
AKC1	LTL19234A	Mollusk Shells	−260	5672 ± 45	4328–4017 cal BC
AKC2	LTL19235A	Mollusk Shells	−50	4931 ± 45	3573–3167 cal BC
AKC3	LTL19236A	Mollusk Shells	−20	4858 ± 45	3482–3074 cal BC
AKC3	LTL19237A	Mollusk Shells	−170	809 ± 45	1341–1598 cal BC
AKC3	LTL19238A	Mollusk Shells	−280	5107 ± 45	3693–3379 cal BC

From the core AKC2, one sample (LTL19235A) was processed with AMS radiocarbon chronology at a depth of −50 cm with age estimation of 3573–3167 cal BC (95.4%, 2 sigma).

From core AKC3, three samples were dated with AMS radiocarbon chronology (LTL19236A, LTL19237A, LTL19238A) at depths of −20 cm, −170 cm and −280 cm, which

provided ages of 3482–3074 cal BC (95.4%, 2 sigma), 1341–1598 cal BC (95.4%, 2 sigma) and 3693–3379 cal BC (95.4%, 2 sigma), respectively. The age provided for sample LTL19237A from core AKC3 at a depth of −170 cm was not adopted as it appeared to be a contamination from the top layers of the core.

5. Discussion

All the measured parameters in the lithological units from core AKC1 showed distinctive patterns, based on which we were able to interpret the palaeoenvironmental conditions at this part of Akrotiri Salt Lake basin during the deposition of sediments of these units (from ~4100 cal BC).

The dominance of *C. torosa* at the base of AKC1, accompanied mainly by marine and mostly epiphytal species tolerant to brackish conditions, indicates a lagoonal environment with marine influence. Upwards, the prevalence of shallow marine taxa pointed to the opening of the lagoon and the formation of a coastal shallow marine environment. This was further supported by the coexistence of *A. tepida* and Miliolidae. The differences in the dominance of the relative abundances of this foraminiferal fauna can be explained by the variations in salinity and organic matter supply. Partly, the presence of the epiphytic *N. lucifuga* indicates the existence of a sheltered bay with seagrass (*Posidonia*) probably providing a substrate for these attached forms.

Grain size, which consisted of fine material, was indicative of a low energy environment (Figure 3). The geochemistry of core AKC1 indicated a relatively stable ratio of gradual Ti/Ca ratios, which represent input of terrestrially sourced lithogenic material from soil erosion from the catchment into the salt lake, with the exception of −160 cm and −30 cm, where there was a rapid increase of Ti/Ca ratios that can be interpreted by the higher input of lithogenic material to this area of the salt lake corresponding to climatic changes or tectonic activation of the area. The Sr/Ca ratio through the core, which can be used as a proxy of shallow marine environmental conditions, showed a stable shallow lake with continuous marine influence with the exception of level −100 cm, in which there is a rapid increase of Sr/Ca ratios most probably as a result of further shoaling of the water depth due to sea level change [14,49,76–78]. Lithological unit LU4a (~3000 BC), in which there was presence of freshwater ostracod taxa, indicated a strong freshwater inflow to the area.

Micropalaeontological assemblages of core AKC2 were marked by the dominance of *C. torosa*, reflecting a shallow lagoonal enviroment, while accompanying fauna indicated marine as well as freshwater influences. Nonetheless, the prevalence of marine epiphytal species, tolerant to salinity fluctuations between 110 cm and 75 cm, pointed to the opening of the lagoon during this interval. The existence of *A. tepida*, a brackish water benthic foraminifer, tolerant to hyposaline and highly schizohaline conditions [26,79], further supported the inferred paleoenvironmental conditions. Towards the top, the high dominance of *Peneroplis planatus* together with *P. pertusus,* which are species living in association with sea grass, distributed through the coastal areas, further support the existence of a shallow, marine environment. *Peneroplis* species together with Miliolidae are associated with salinities of 34–68‰, temperatures of 17–27 °C, and fine sand [80]. Furthermore, in this part of the core, the relative abundance of *Ammonia beccari* increased, indicating a rather augmented supply of organic matter (e.g., [79]).

The grain size consisted mainly of fine sand size particles showing a low energy lagoonal environment. The geochemistry of the core AKC2 was fairly stable with the exception of Ti/Ca ratios rising at −95 cm, indicating a higher input of lithogenic material to the Salt Lake, probably from climatic variation and in accordance with micropalaeontological assemblages, indicating an opening of the lagoon (before 3500 BC). A peak of the Sr/Ca ratio at −70 cm also indicated a further shoaling of the water depth of the Salt Lake, more likely due to tectonic action.

Ostracod assemblages throughout core AKC3 (Figure 4) indicated a shallow lagoonal environment with continuous marine influence. The exception of LU3c (145–65 cm), in

which ostracod taxa assemblages were nearly monospecific, and *C. torosa* and freshwater species were scarcely present, indicated the isolation of that part of the lagoon.

The location of the core and the data from LU3c suggest that the spit at the east of the Salt Lake, which was already formed at that time period (between ~3600 and 3000 BC), increased significantly, resulting in the isolation of that part of the salt lake from the sea. The geochemical analysis of the core indicated stable rates of Ti/Ca ratios (with the exception of −206 cm, −120 cm and −55 cm), in which there was higher input of lithogenic material to this area of the Salt Lake, corresponding to climatic change or tectonic activation of the area. Sr/Ca ratios were stable along the core with the exception of level −65 cm, in which a high peak of Sr/Ca ratios was observed. The Sr/Ca peak indicated a shoaling of the water depth of the Salt Lake, which corresponds to the isolation of this part of the salt lake from the sea at that time period (~3200 BC).

The ages provided by AMS radiocarbon in correlation with the analyses of the cores showed a high sediment deposition rate to the north-east side of the Salt Lake and a lower deposition rate at the center-east side of the salt lake. This is in direct connection with the data, suggesting a development of a spit from the north-east to the south-east side of the area. We suggest that the north-east side of the lake was isolated from the sea earlier in time. The east central area was isolated from the sea much later in time and, as a result, wave action delayed the accumulation of sediments.

Historical maps, mainly from the Venetian period (1500–1600 AD), depict the Salt Lake isolated from the sea (Figure 5). The maps point out the connection between the lake and the sea by a channel to the east (Figure 1). This is also identified by historical texts which refer to an artificial channel [81]. The opening of the channel can explain the marine influence of the Salt Lake, which was observed on the top layers of the cores. The Kouris river is also depicted flowing directly to the north side of the lake, but there are no other data to suggest this.

Palaeogeographic Reconstruction

With the combination of all the data retrieved from the core analysis, field investigation, remote sensing and GIS analysis, as well as historical sources, we propose the palaeogeographic evolution of the study area.

The development of the Salt Lake initially started during the Lower Holocene as an open bay from the east. The tombolo on the west was already formed by the discharged material from the Kouris river. Sand to the north-east started to accumulate, forming an early sand barrier. At approximately 6000–4000 years BP, the barrier moved further south, forming an extended spit which had, as a result, a semi open lagoon (Figure 6a). The north-east part of the lagoon was mostly protected from the sea, and a low energy environment was established. This caused, as a result, the deposition of finer material at that part of the lagoon and the freshwater influence to be more profound. At the center of the semi open lagoon, deposition was continues at low energy conditions because of the distance from the opening to the sea.

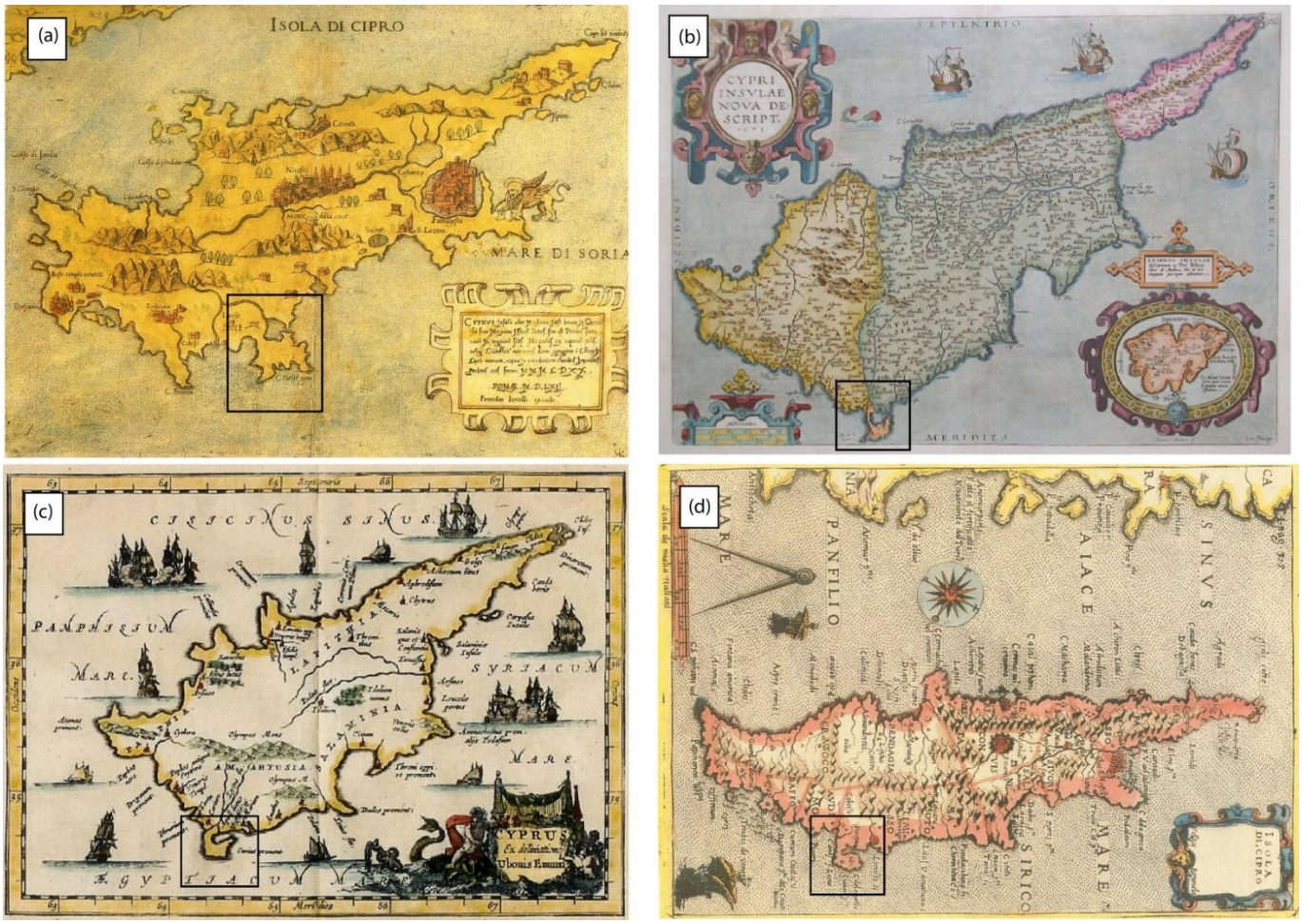

Figure 5. Historical maps of Cyprus. The study area is within the black square. (**a**) Ferrando Bertalli (1562), Isola Di Cipro. (**b**) Abraham Ortelius (1612) Cypri insulae nova descript. (**c**) Philipp Cluverius. (1682) Cyprus Ex deliniatione Ubonis Emmii. (**d**) Felice Brunello (1570) Isola di Cipro.

During the period from 4000–2000 years BP, the spit extended and reached the south mainland, creating a narrow tombolo to the east that resulted in the closure of the lagoon (Figure 6b). The restriction of the lagoon from the direct influence of the sea created low energy conditions and the deposition of fine grain sediments. The freshwater influence was also more profound over the entire length of the lagoon, not only the north-east part. The narrow tombolo was developed enough to restrict the lagoon from the sea, but during high energy events the sea was able to overstep the tombolo and affect the lagoon.

During the last two millennia, the eastern tombolo extended further in length, creating a wide barrier between the closed lagoon and the sea (Figure 6c). At this stage, the anthropogenic influence was maximized in the area and the development of a channel (18 m wide) at the east (Figure 1), which connected the lagoon to the sea, established a new cycle of marine influence at the inner area of the lagoon. Because of the low topography of the eastern tombolo a direct connection of the sea with the lagoon occurred during high energy events (storms).

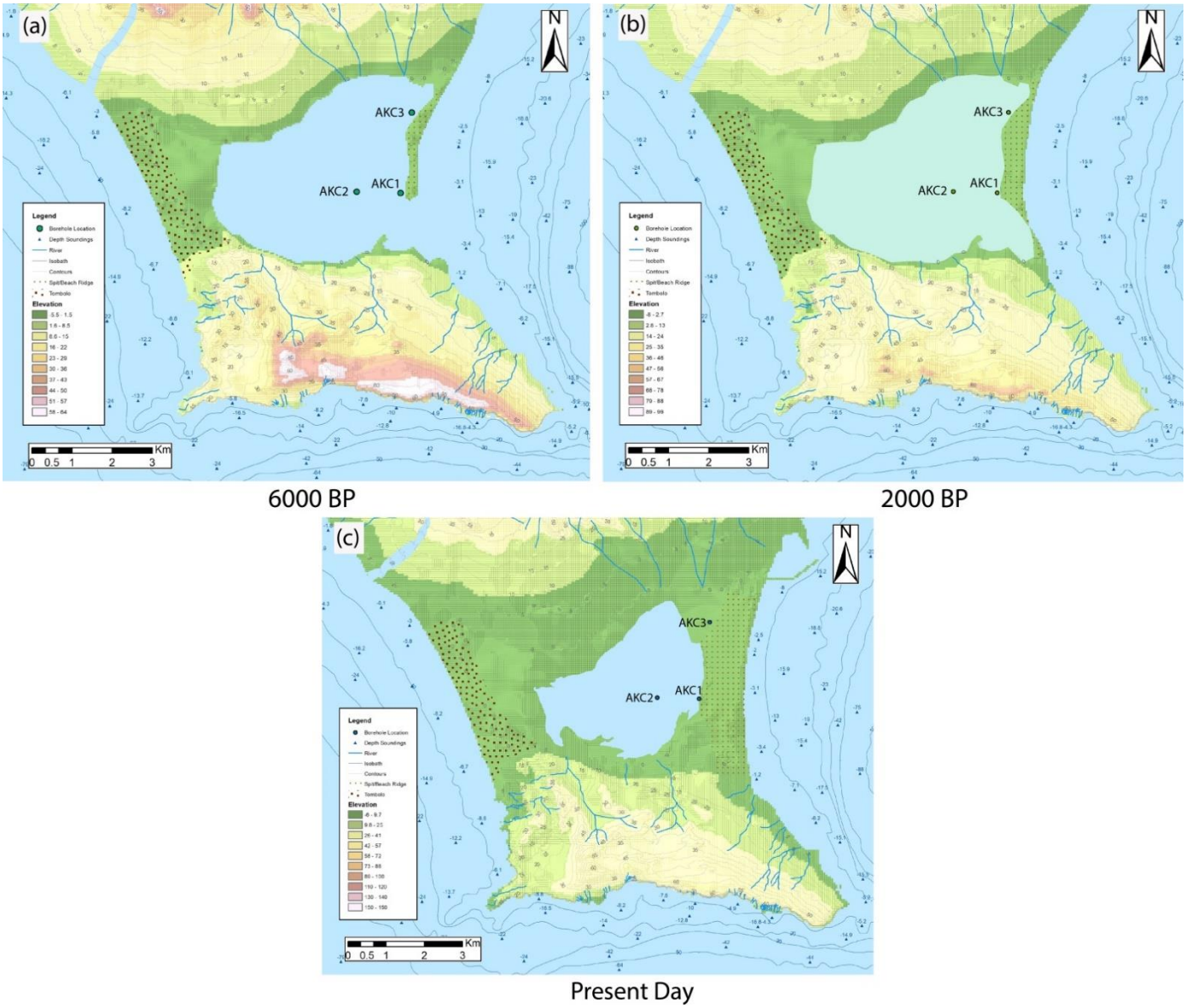

Figure 6. Palaeogeographic reconstruction of the Akrotiri peninsula. (**a**) Palaeogeographic reconstruction of study area ~6000 BP. (**b**) Palaeogeography and paleocoastline ~2000 BP. (**c**) Present state of the study area.

6. Conclusions

This study provides data on the middle and upper Holocene palaeoenvironmental development of the Akrotiri Salt Lake. The palaeoenvironmental changes were driven by sea level and climate variations and tectonic actions that occurred during the middle-upper part of the Holocene. Sediment cores AKC1, AKC2 and AKC3 revealed the depositional environments in the Salt Lake.

The Salt Lake developed in three phases, from an open bay (6000 to 4000 years BP) to a semi closed lagoon (4000 to 2000 years BP) and finally to a restricted lagoon (2000 years to the present day). During the entire time of the evolution of the Salt Lake, the influence of the sea was significant, either by direct connection, high energy events (storms) and/or anthropogenic activity.

The combined use of geochemical, sedimentological and palaeontological proxies, combined with radiocarbon dating, are valuable indicators for the interpretation of past environments in these types of geological setting and can shed light on the reconstruction of palaeogeographic evolution.

Author Contributions: Conceptualization, M.P. and N.E.; methodology, M.P., N.E., H.D. and T.T.; validation, M.P., N.E., H.D., T.T., F.S. and L.B.; investigation, M.P., N.E., F.S. and L.B.; writing—original draft preparation, M.P. and N.E.; review and editing, H.D., T.T., F.S. and L.B.; supervision, N.E. and M.P. All authors have read and agreed to the published version of the manuscript.

Funding: This research was partly funded by Honor Frost Foundation, 10 Carlton House Terrace, London SW1Y 5AH, "Small Grant Award".

Institutional Review Board Statement: Not applicable.

Informed Consent Statement: Not applicable.

Acknowledgments: The authors would like to thank British Sovereign Bases Areas Administration (SBAA) and personnel for their support to this project. The authors would like to thank Eleana Karkani and Giannis Saitis for their contribution to the project.

Conflicts of Interest: The authors declare no conflict of interest.

Appendix A

Table A1. Handheld XRF geochemistry of the studied cores (Mg to Fe values in ppm).

Core	Depth	Mg	Al	Si	P	S	K	Rb	Ca	Sr	Ti	V	Cr	Mn	Fe
AKC1	34	0	5268	40947	4592	503	797	3	116976	477	2548	57	198	742	31799
AKC1	42	0	6291	50019	2869	0	1072	5	92045	348	1895	47	197	664	29854
AKC1	60	8044	8753	56525	3192	221	904	4	100739	361	1756	62	229	685	29100
AKC1	94	7551	3663	33386	2646	691	1395	7	133975	622	1440	43	313	511	17202
AKC1	105	0	2986	23993	3679	534	532	4	179338	1367	1111	44	259	404	12870
AKC1	145	7777	3325	39464	2532	230	510	3	142114	738	1200	42	155	401	13940
AKC1	172	0	8868	55585	4814	241	1022	5	106482	389	2699	71	208	803	31127
AKC1	189	0	5088	37798	2852	478	772	4	127823	543	2644	60	498	661	25659
AKC1	198	0	5543	45500	3457	1734	561	4	125825	668	1609	40	366	532	20796
AKC1	227	0	4663	39631	3350	2135	503	4	126617	685	1356	42	332	477	17537
AKC1	231	0	3087	39551	1726	971	363	3	129696	582	1163	36	179	485	16248
AKC1	237	0	3963	32224	3051	2354	727	5	131080	735	1772	52	360	540	17213
AKC1	273	0	5288	45357	4193	2185	819	5	155471	903	1295	0	375	441	17371
	Depth														
AKC2	3	14253	7216	42132	5906	1116	478	4	126697	692	1323	40	147	540	20886
AKC2	17	0	4879	39381	3725	1310	523	3	129421	595	2683	63	421	927	33266
AKC2	27	0	4209	36401	3571	1219	675	4	144540	1086	1913	46	304	732	22093
AKC2	39	0	3665	28489	3929	955	871	3	175881	1544	923	44	130	586	12547
AKC2	49	0	2871	26779	3997	530	1466	5	161349	2438	2602	55	1085	679	21688
AKC2	55	0	1464	17630	4059	152	1234	0	190345	3608	1028	50	329	454	12999
AKC2	63	0	3964	32872	1948	0	2001	5	137748	1044	2017	59	2867	707	30501
AKC2	73	0	6971	41100	2102	0	5676	14	92218	456	2050	67	5089	632	40537
AKC2	90	0	1964	18389	2159	0	817	4	185092	398	1174	56	2197	530	20594
AKC2	99	0	2133	24822	2796	0	87	3	176893	411	1176	50	1212	537	21598

Table A1. *Cont.*

Core	Depth	Mg	Al	Si	P	S	K	Rb	Ca	Sr	Ti	V	Cr	Mn	Fe
AKC2	130	0	897	18736	2821	0	102	2	188481	392	1050	34	1002	437	16133
AKC2	140	0	821	23206	3079	0	0	1	185563	427	965	53	1484	439	15681
AKC2	150	0	1165	23442	3273	0	0	2	179240	461	820	36	865	452	17613
	Depth														
AKC3	18	6508	5359	43124	1446	114	829	6	130757	1047	2885	56	474	714	25609
AKC3	52	0	8527	65555	880	0	2988	9	63318	582	7505	109	2029	789	40666
AKC3	60	0	4134	41211	1733	0	1468	5	145175	2775	2026	66	252	448	17628
AKC3	83	8248	9071	83286	1969	0	2095	8	84035	850	4222	77	992	804	36400
AKC3	93	8293	7858	59971	1164	233	2792	10	89246	517	4085	86	1268	945	36525
AKC3	105	0	8005	80674	980	0	2163	8	65554	260	5884	80	1810	833	38817
AKC3	116	7656	10431	66676	1009	0	3036	10	69698	273	7619	132	2621	987	48262
AKC3	144	0	7810	68622	1427	66	1675	5	66747	263	5522	94	1600	733	36299
AKC3	153	0	4628	51487	3817	580	925	6	119058	512	2361	54	468	608	19321
AKC3	172	9852	5896	52601	8640	734	1415	8	95048	480	2441	51	531	605	23276
AKC3	199	0	6676	41357	14205	620	2942	9	86561	642	5212	70	1845	931	32696
AKC3	220	6722	9632	79711	2377	68	1400	6	81403	456	5086	90	2190	867	38840
AKC3	240	0	5796	53375	1408	155	1321	6	101895	877	2687	70	707	664	26359
AKC3	258	0	7900	61899	734	0	1440	6	80328	485	7692	107	2449	880	39474
AKC3	280	0	4578	36709	1802	307	1217	5	138447	945	3815	69	1807	802	29418
AKC3	285	7148	4798	45351	2367	161	380	4	122317	717	2705	87	1372	579	22136
AKC3	294	0	7689	68957	789	0	748	5	77960	356	4570	82	963	706	32716
AKC3	330	6002	10414	88774	308	60	2475	8	42796	220	8612	150	3061	808	45582
AKC3	338	0	11312	124005	149	58	1342	7	31935	125	2595	68	454	569	26735

Table A2. Handheld XRF geochemistry of the studied cores (Co to U values in ppm).

Core	Depth	Co	Ni	Cu	Zn	As	Se	Y	Zr	Nb	Mo	Ag	Cd	Sn	Sb	W	Au	Hg	Pb	Bi	Th	U
AKC1	34	0	91	28	28	3	0	13	25	0	0	0	0	0	0	0	0	0	5	0	0	0
AKC1	42	0	95	23	27	3	0	13	22	0	0	0	0	0	0	0	0	0	0	0	0	0
AKC1	60	0	94	23	29	3	0	12	20	0	0	0	0	0	0	0	0	0	0	8	0	0
AKC1	94	0	109	24	22	6	0	11	26	0	0	0	0	0	0	0	0	0	3	0	0	0
AKC1	105	0	102	18	16	10	0	11	18	0	0	0	0	0	0	0	0	0	0	0	0	0
AKC1	145	0	110	12	17	4	0	12	20	0	0	0	0	0	0	0	0	0	0	0	0	0
AKC1	172	0	100	25	38	3	0	12	23	0	0	0	0	0	0	0	0	0	0	0	0	0
AKC1	189	0	120	22	33	3	0	12	19	0	0	0	0	0	0	0	0	0	4	0	0	0
AKC1	198	0	155	19	24	9	0	11	18	0	0	0	0	0	0	0	0	0	0	8	0	0
AKC1	227	0	125	17	19	7	0	10	17	0	0	0	0	0	0	0	0	0	0	0	0	0
AKC1	231	0	102	18	22	8	0	10	18	0	0	0	0	0	0	0	0	0	0	0	0	0
AKC1	237	0	131	22	22	9	0	10	33	0	0	0	0	0	0	0	0	0	0	12	0	0
AKC1	273	0	87	19	18	16	0	14	26	0	0	0	0	0	0	0	0	0	5	0	0	0
	Depth																					
AKC2	3	0	93	23	21	6	0	9	20	0	0	0	0	0	0	0	0	0	3	14	0	0
AKC2	17	0	101	20	26	5	0	12	21	0	0	0	0	0	0	0	0	0	5	8	0	0
AKC2	27	0	103	15	22	4	0	8	23	0	0	0	0	0	0	0	0	0	5	0	0	0
AKC2	39	0	77	16	16	4	0	7	17	0	0	0	0	0	0	0	0	0	4	0	0	0
AKC2	49	0	122	19	28	4	0	8	37	0	0	0	0	0	0	0	0	0	6	0	10	0
AKC2	55	0	78	12	13	4	0	6	31	0	0	0	0	0	0	0	0	0	0	0	0	0
AKC2	63	0	195	20	36	3	0	14	22	0	0	0	0	0	0	0	4	0	4	0	0	0
AKC2	73	0	245	37	57	2	0	13	53	0	0	0	0	0	0	0	0	0	3	10	0	0
AKC2	90	0	196	22	27	0	0	7	12	0	0	0	0	0	0	0	0	5	4	0	0	0
AKC2	99	0	304	21	22	2	0	6	9	0	0	0	0	0	0	0	0	0	0	0	0	0
AKC2	130	0	221	18	17	3	0	6	11	0	0	0	0	0	0	0	0	6	0	0	0	0
AKC2	140	0	222	24	17	3	0	5	10	0	0	0	0	0	0	0	0	0	0	0	0	0

Table A2. *Cont.*

Core	Depth	Co	Ni	Cu	Zn	As	Se	Y	Zr	Nb	Mo	Ag	Cd	Sn	Sb	W	Au	Hg	Pb	Bi	Th	U
AKC2	150	0	246	21	18	3	0	5	11	0	0	0	0	0	0	0	0	0	0	0	0	0
	Depth																					
AKC3	18	0	103	22	27	5	0	19	29	0	0	0	0	0	0	0	0	0	3	9	0	0
AKC3	52	0	103	23	42	4	0	23	49	0	0	0	0	0	0	0	0	5	3	0	0	0
AKC3	60	0	61	15	20	6	0	13	29	0	0	0	0	0	0	0	0	0	0	0	0	0
AKC3	83	0	86	19	33	3	0	20	43	0	0	0	0	0	0	0	0	5	6	0	0	0
AKC3	93	0	97	26	36	4	0	20	64	0	0	0	0	0	0	0	0	6	4	9	0	0
AKC3	105	0	100	20	36	3	0	24	34	0	0	0	0	0	0	0	0	0	4	0	0	0
AKC3	116	0	99	26	47	4	0	23	48	0	0	0	0	0	0	0	0	0	3	14	0	0
AKC3	144	0	76	17	35	4	0	21	45	0	0	0	0	0	0	0	0	0	0	13	0	0
AKC3	153	0	48	14	22	3	0	18	29	0	0	0	0	0	0	0	0	0	3	0	0	0
AKC3	172	0	71	22	28	5	0	17	44	0	0	0	0	0	0	0	0	0	10	9	0	0
AKC3	199	0	101	32	53	4	0	17	92	0	0	0	0	0	0	0	0	0	24	15	0	0
AKC3	220	0	96	19	39	4	0	23	61	0	0	0	0	0	0	0	0	6	0	0	0	0
AKC3	240	0	87	23	27	5	0	19	36	0	0	0	0	0	0	0	0	5	3	9	0	0
AKC3	258	0	103	22	37	2	0	21	82	0	0	0	0	0	0	0	0	0	5	0	0	0
AKC3	280	0	96	20	33	6	0	17	34	0	0	0	0	0	0	0	0	0	0	0	0	0
AKC3	285	0	117	19	23	6	0	17	29	0	0	0	0	0	0	0	0	5	0	0	0	0
AKC3	294	0	115	18	29	3	0	18	31	0	0	0	0	0	0	0	0	0	0	18	0	0
AKC3	330	0	104	23	46	5	0	19	65	0	0	0	0	0	0	0	0	5	3	14	0	0
AKC3	338	0	90	19	27	2	0	19	32	0	0	0	0	0	0	0	0	0	3	8	0	0

Table A3. Handheld XRF Ti/Ca, Sr/Ca ratios.

Core	Depth	Ca	Ti	Sr	Ti/Ca	Sr/Ca
AKC1	34	116,976	2548	477	0.021782	0.004078
AKC1	42	92,045	1895	348	0.020588	0.003781
AKC1	60	100,739	1756	361	0.017431	0.003584
AKC1	94	133,975	1440	622	0.010748	0.004643
AKC1	105	179,338	1111	1367	0.006195	0.007622
AKC1	145	142,114	1200	738	0.008444	0.005193
AKC1	172	106,482	2699	389	0.025347	0.003653
AKC1	189	127,823	2644	543	0.020685	0.004248
AKC1	198	125,825	1609	668	0.012788	0.005309
AKC1	227	126,617	1356	685	0.010709	0.00541
AKC1	231	129,696	1163	582	0.008967	0.004487
AKC1	237	131,080	1772	735	0.013518	0.005607
AKC1	273	155,471	1295	903	0.00833	0.005808
Core	Depth	Ca	Ti	Sr	Ti/Ca	Sr/Ca
AKC2	3	126,697	1323	692	0.010442	0.005462
AKC2	17	129,421	2683	595	0.020731	0.004597
AKC2	27	144,540	1913	1086	0.013235	0.007513
AKC2	39	175,881	923	1544	0.005248	0.008779
AKC2	49	161,349	2602	2438	0.016127	0.01511
AKC2	55	190,345	1028	3608	0.005401	0.018955
AKC2	63	137,748	2017	1044	0.014643	0.007579
AKC2	73	92,218	2050	456	0.02223	0.004945
AKC2	90	185,092	1174	398	0.006343	0.00215
AKC2	99	176,893	1176	411	0.006648	0.002323
AKC2	130	188,481	1050	392	0.005571	0.00208
AKC2	140	185,563	965	427	0.0052	0.002301
AKC2	150	179,240	820	461	0.004575	0.002572
Core	Depth	Ca	Ti	Sr	Ti/Ca	Sr/Ca
AKC3	18	130,757	2885	1047	0.022064	0.008007
AKC3	52	63,318	7505	582	0.118529	0.009192
AKC3	60	145,175	2026	2775	0.013956	0.019115
AKC3	83	84,035	4222	850	0.050241	0.010115
AKC3	93	89,246	4085	517	0.045772	0.005793
AKC3	105	65,554	5884	260	0.089758	0.003966
AKC3	116	69,698	7619	273	0.109314	0.003917
AKC3	144	66,747	5522	263	0.08273	0.00394
AKC3	153	119,058	2361	512	0.019831	0.0043
AKC3	172	95,048	2441	480	0.025682	0.00505
AKC3	199	86,561	5212	642	0.060212	0.007417
AKC3	220	81,403	5086	456	0.062479	0.005602
AKC3	240	101,895	2687	877	0.02637	0.008607
AKC3	258	80,328	7692	485	0.095757	0.006038
AKC3	280	138,447	3815	945	0.027556	0.006826
AKC3	285	122,317	2705	717	0.022115	0.005862
AKC3	294	77,960	4570	356	0.05862	0.004566
AKC3	330	42,796	8612	220	0.201234	0.005141
AKC3	338	31,935	2595	125	0.081259	0.003914

Table A4. Relative frequencies of the ostracod species in the studied samples of AKC1 (1 to 135 cm).

Depth (cm)	1–5	15–20	30–35	40–45	50–55	60–65	70–75	80–85	90–95	100–105	110–115	120–125	130–135
Cyprideis torosa	54.55	33.33	0.00	0.00	16.67	6.52	20.31	7.41	4.05	20.70	19.15	11.22	12.68
A. convexa	0.00	0.00	0.00	0.00	0.00	4.35	0.00	0.00	0.00	1.16	2.48	0.00	0.00
***Aurila* spp.**	0.00	0.00	0.00	0.00	0.00	0.00	4.69	0.00	0.58	2.56	0.71	3.06	9.86
Aurila woodwardii	0.00	18.18	0.00	0.00	0.00	0.00	1.56	0.00	4.05	2.56	3.90	7.14	2.82
***Phlyctenophora* sp.**	18.18	24.24	0.00	0.00	0.00	13.04	3.13	5.93	4.91	11.63	20.21	5.10	4.23
Heterocypris salina	0.00	0.00	0.00	0.00	83.33	8.70	21.88	2.96	1.45	0.47	0.71	1.02	0.00
***Limnocythere* sp.**	0.00	0.00	0.00	0.00	0.00	0.00	1.56	0.00	0.00	0.00	0.00	0.00	0.00
Xestoleberis communis	0.00	6.06	0.00	0.00	0.00	19.57	15.63	10.37	16.18	7.21	7.80	6.12	9.86
***Xestoleberis* spp.**	0.00	0.00	0.00	0.00	0.00	0.00	1.56	0.00	0.58	0.00	0.00	0.00	1.41
Basslerites berchoni	0.00	0.00	0.00	0.00	0.00	6.52	0.00	4.44	3.47	2.79	3.55	2.04	5.63
Loxoconcha affinis	0.00	9.09	0.00	0.00	0.00	17.39	18.75	28.15	49.13	37.67	24.47	25.51	9.86
***Loxoconcha* spp.**	0.00	0.00	0.00	0.00	0.00	0.00	0.00	4.44	1.45	0.47	0.00	3.06	5.63
***Leptocythere* sp.**	0.00	0.00	0.00	0.00	0.00	0.00	0.00	6.67	3.47	2.33	4.26	0.00	1.41
***Pontocythere* spp.**	0.00	0.00	0.00	0.00	0.00	4.35	0.00	1.48	2.02	1.86	2.83	3.06	4.23
***Urocythereis* sp.**	27.27	0.00	0.00	0.00	0.00	8.70	0.00	5.19	0.87	1.16	2.48	4.08	4.23
***Semicytherura* sp.**	0.00	0.00	0.00	0.00	0.00	0.00	0.00	6.67	0.58	0.47	0.00	4.08	7.04
***Hemicytherura* sp.**	0.00	0.00	0.00	0.00	0.00	2.17	0.00	0.00	0.00	0.00	0.00	0.00	0.00
***Callistocythere* sp.**	0.00	0.00	0.00	0.00	0.00	0.00	3.13	0.00	0.00	1.40	0.00	0.00	0.00
***Carinocythereis* sp.**	0.00	0.00	0.00	0.00	0.00	0.00	0.00	0.00	0.58	0.00	0.00	1.02	0.00
***Hiltermannicythere* sp.**	0.00	9.09	0.00	0.00	0.00	4.35	0.00	6.67	2.31	1.16	2.13	3.06	4.23
***Quadracythere* sp.**	0.00	0.00	0.00	0.00	0.00	0.00	0.00	0.00	0.58	0.47	0.35	0.00	0.00
***Cytheretta* sp.**	0.00	0.00	0.00	0.00	0.00	0.00	0.00	0.00	2.02	0.93	0.35	2.04	4.23
***Cytherella* sp.**	0.00	0.00	0.00	0.00	0.00	0.00	0.00	2.22	0.29	1.16	0.71	0.00	4.23
***Eucytherura* sp.**	0.00	0.00	0.00	0.00	0.00	0.00	0.00	0.00	0.00	0.00	0.00	0.00	0.00
***Sagmatocythere* sp.**	0.00	0.00	0.00	0.00	0.00	0.00	4.69	5.19	1.45	1.86	2.48	12.24	4.23
***Triebelina* sp.**	0.00	0.00	0.00	0.00	0.00	0.00	0.00	0.00	0.00	0.00	0.35	0.00	0.00
not identified	0.00	0.00	0.00	0.00	0.00	4.35	3.13	2.22	0.00	0.00	1.06	6.12	4.23

Table A5. Relative frequencies of the ostracod species in the studied samples of AKC1 (140 to 265 cm).

Depth (cm)	140–145	145–150	155–160	170–175	180–185	190–195	200–205	210–215	220–225	230–235	240–245	250–255	260–265
Cyprideis torosa	11.43	7.41	0.00	0.00	0.00	28.57	8.33	0.00	25.00	80.77	30.53	54.05	7.84
A. convexa	0.00	0.00	0.00	0.00	0.00	14.29	0.00	0.00	0.00	0.00	0.00	0.00	0.00
***Aurila* spp.**	8.57	7.41	0.00	33.33	10.00	9.52	8.33	30.00	0.00	0.00	0.00	0.00	0.00
Aurila woodwardii	0.00	0.00	0.00	0.00	0.00	0.00	8.33	0.00	0.00	0.00	20.00	16.22	21.57
***Phlyctenophora* sp.**	0.00	37.04	0.00	0.00	10.00	0.00	8.33	10.00	0.00	0.00	2.11	0.00	9.80
Heterocypris salina	0.00	3.70	0.00	0.00	0.00	0.00	0.00	0.00	25.00	0.00	0.00	0.00	0.00
***Limnocythere* sp.**	0.00	0.00	0.00	0.00	0.00	0.00	0.00	0.00	0.00	0.00	0.00	0.00	0.00
Xestoleberis communis	0.00	11.11	0.00	0.00	20.00	0.00	8.33	0.00	0.00	1.28	8.42	5.41	1.96
***Xestoleberis* spp.**	5.71	0.00	0.00	0.00	0.00	9.52	0.00	0.00	0.00	0.00	0.00	0.00	0.00
Basslerites berchoni	0.00	0.00	0.00	0.00	0.00	0.00	4.17	0.00	0.00	0.00	18.95	0.00	39.22
Loxoconcha affinis	22.86	14.81	0.00	33.33	0.00	0.00	0.00	20.00	0.00	2.56	3.16	13.51	15.69
***Loxoconcha* spp.**	0.00	0.00	0.00	0.00	10.00	0.00	0.00	0.00	0.00	0.00	2.11	0.00	0.00
***Leptocythere* sp.**	0.00	0.00	0.00	0.00	0.00	0.00	4.17	0.00	0.00	2.56	1.05	0.00	0.00
***Pontocythere* spp.**	11.43	0.00	0.00	0.00	0.00	0.00	8.33	10.00	12.50	6.41	4.21	0.00	0.00
***Urocythereis* sp.**	8.57	0.00	100.00	0.00	10.00	9.52	4.17	0.00	0.00	0.00	0.00	0.00	0.00
***Semicytherura* sp.**	5.71	3.70	0.00	0.00	10.00	9.52	8.33	10.00	0.00	0.00	0.00	0.00	0.00
***Hemicytherura* sp.**	0.00	0.00	0.00	0.00	0.00	0.00	0.00	0.00	0.00	0.00	1.05	0.00	0.00
***Callistocythere* sp.**	5.71	0.00	0.00	0.00	0.00	0.00	0.00	0.00	0.00	2.56	0.00	0.00	3.92
***Carinocythereis* sp.**	2.86	0.00	0.00	0.00	0.00	0.00	0.00	10.00	0.00	0.00	0.00	0.00	0.00
***Hiltermannicythere* sp.**	8.57	3.70	0.00	0.00	0.00	9.52	8.33	0.00	25.00	0.00	6.32	5.41	0.00
***Quadracythere* sp.**	0.00	0.00	0.00	0.00	0.00	0.00	0.00	0.00	0.00	0.00	0.00	0.00	0.00
***Cytheretta* sp.**	0.00	0.00	0.00	33.33	30.00	4.76	0.00	0.00	0.00	0.00	0.00	0.00	0.00
***Cytherella* sp.**	0.00	11.11	0.00	0.00	0.00	0.00	0.00	0.00	0.00	0.00	2.11	0.00	0.00
***Eucytherura* sp.**	0.00	0.00	0.00	0.00	0.00	0.00	0.00	0.00	0.00	0.00	0.00	0.00	0.00
***Sagmatocythere* sp.**	2.86	0.00	0.00	0.00	0.00	4.76	12.50	10.00	12.50	2.56	0.00	5.41	0.00
***Triebelina* sp.**	2.86	0.00	0.00	0.00	0.00	0.00	0.00	0.00	0.00	0.00	0.00	0.00	0.00
not identified	2.86	0.00	0.00	0.00	0.00	0.00	8.33	0.00	0.00	1.28	0.00	0.00	0.00

Table A6. Relative frequencies of the ostracod species in the studied samples of AKC2.

Depth (cm)	5–10	30–35	35–40	45–50	55–60	65–70	75–80	85–90	95–100	105–110	115–120	125–130	140–145	155–160	170–175	180–185	190–195
Cyprideis torosa	78.13	76.67	83.33	83.33	99.71	87.50	11.11	0.76	0.00	0.00	0.00	0.00	0.00	0.00	0.00	93.69	85.29
Aurila woodwardii	0.00	0.00	0.00	1.67	0.00	0.00	27.78	57.25	100.00	0.00	0.00	0.00	0.00	0.00	0.00	0.00	2.94
Phlyctenophora **sp.**	9.38	13.33	16.67	3.33	0.00	0.00	0.00	0.00	0.00	0.00	0.00	0.00	0.00	0.00	0.00	1.80	4.41
Heterocypris salina	0.00	0.00	0.00	0.00	0.19	0.00	0.00	0.00	0.00	0.00	0.00	0.00	0.00	0.00	0.00	0.90	1.47
Xestoleberiscommunis	0.00	0.00	0.00	1.67	0.00	7.81	11.11	33.59	0.00	0.00	0.00	0.00	0.00	0.00	0.00	0.00	0.00
Xestoleberis **sp.**	0.00	0.00	0.00	0.00	0.00	0.00	0.00	0.76	0.00	0.00	0.00	0.00	0.00	0.00	0.00	0.00	0.00
Loxoconcha affinis	3.13	0.00	0.00	8.33	0.00	0.00	0.00	0.76	0.00	0.00	0.00	0.00	0.00	0.00	0.00	0.00	0.00
Loxoconcha **sp.**	0.00	0.00	0.00	0.00	0.00	0.00	0.00	6.11	0.00	0.00	0.00	0.00	0.00	0.00	0.00	0.00	0.00
Urocythereis **sp.**	9.38	3.33	0.00	1.67	0.00	3.13	33.33	0.76	0.00	0.00	0.00	0.00	0.00	0.00	0.00	3.60	4.41
Semicytherura **sp.**	0.00	0.00	0.00	0.00	0.00	0.00	0.00	0.00	0.00	0.00	0.00	0.00	0.00	0.00	0.00	0.00	1.47
not identified	0.00	6.67	0.00	0.00	0.10	1.56	16.67	0.00	0.00	0.00	0.00	0.00	0.00	0.00	0.00	0.00	0.00

Table A7. Relative frequencies of the ostracod species in the studied samples of AKC3 (5 to 150 cm).

Depth (cm)	5–10	15–20	25–30	35–40	45–50	55–60	65–70	75–80	85–90	95–100	105–110	115–120	125–130	135–140	145–150
Cyprideis torosa	31.09	21.80	66.67	0.00	0.00	6.94	99.32	97.98	99.80	93.33	100.00	60.00	40.00	56.23	7.74
A. convexa	0.00	0.00	0.00	0.00	0.00	0.00	0.00	0.00	0.00	0.00	0.00	0.00	0.00	0.00	0.00
Aurila **spp.**	0.00	0.00	0.00	0.00	7.14	0.00	0.00	0.00	0.20	0.00	0.00	0.00	0.00	0.00	0.00
Aurila woodwardii	9.62	6.02	0.00	0.00	0.00	90.28	0.00	0.00	0.00	0.83	0.00	40.00	60.00	31.78	56.77
Phlyctenophora **sp.**	21.79	23.31	33.33	0.00	0.00	0.00	0.68	0.00	0.00	0.00	0.00	0.00	0.00	0.98	8.39
Heterocypris salina	0.00	0.00	0.00	0.00	0.00	0.00	0.00	0.00	0.00	5.00	0.00	0.00	0.00	0.00	0.00
Xestoleberis **communis**	3.85	12.78	0.00	0.00	28.57	1.39	0.00	1.01	0.00	0.00	0.00	0.00	0.00	0.98	1.94
Xestoleberis **spp.**	0.64	0.00	0.00	0.00	0.00	0.00	0.00	0.00	0.00	0.00	0.00	0.00	0.00	0.49	7.74
Basslerites berchoni	0.96	1.88	0.00	0.00	0.00	0.00	0.00	0.00	0.00	0.00	0.00	0.00	0.00	0.00	0.00
Loxoconcha affinis	20.19	27.44	0.00	0.00	28.57	0.00	0.00	0.00	0.00	0.00	0.00	0.00	0.00	1.96	10.97
Loxoconcha **sp.**	3.53	0.00	0.00	0.00	0.00	0.00	0.00	0.00	0.00	0.00	0.00	0.00	0.00	0.00	0.00
Leptocythere **sp.**	3.21	2.26	0.00	0.00	0.00	0.00	0.00	0.00	0.00	0.00	0.00	0.00	0.00	1.22	0.00
Urocythereis **sp.**	0.32	0.00	0.00	0.00	14.29	0.00	0.00	1.01	0.00	0.00	0.00	0.00	0.00	0.49	3.23
Pontocythere **spp.**	0.00	0.00	0.00	0.00	0.00	0.00	0.00	0.00	0.00	0.00	0.00	0.00	0.00	0.00	0.00

Table A7. *Cont.*

Depth (cm)	5–10	15–20	25–30	35–40	45–50	55–60	65–70	75–80	85–90	95–100	105–110	115–120	125–130	135–140	145–150
***Callistocythere* sp.**	0.32	0.00	0.00	0.00	0.00	0.00	0.00	0.00	0.00	0.00	0.00	0.00	0.00	0.00	0.00
***Hiltermannicythere* sp.**	0.32	0.00	0.00	0.00	7.14	0.00	0.00	0.00	0.00	0.00	0.00	0.00	0.00	4.89	2.58
***Cytheretta* sp.**	0.32	0.00	0.00	0.00	0.00	0.00	0.00	0.00	0.00	0.00	0.00	0.00	0.00	0.00	0.00
***Cytherella* sp.**	0.64	0.00	0.00	0.00	0.00	0.00	0.00	0.00	0.00	0.00	0.00	0.00	0.00	0.00	0.00
***Eucytherura* sp.**	0.00	0.00	0.00	0.00	0.00	0.00	0.00	0.00	0.00	0.00	0.00	0.00	0.00	0.00	0.00
***Propontocypris* sp.**	0.00	0.00	0.00	0.00	0.00	0.00	0.00	0.00	0.00	0.00	0.00	0.00	0.00	0.00	0.00
***Sagmatocythere* sp.**	0.00	0.38	0.00	0.00	7.14	0.00	0.00	0.00	0.00	0.00	0.00	0.00	0.00	0.00	0.00
***Triebelina* sp.**	0.00	0.00	0.00	0.00	0.00	0.00	0.00	0.00	0.00	0.00	0.00	0.00	0.00	0.00	0.00
***Semicytherura* sp.**	2.24	3.76	0.00	0.00	0.00	0.00	0.00	0.00	0.00	0.00	0.00	0.00	0.00	0.98	0.65
not identified	0.96	0.38	0.00	0.00	7.14	1.39	0.00	0.00	0.00	0.00	0.00	0.00	0.00	0.00	0.00

Table A8. Relative frequencies of the ostracod species in the studied samples of AKC3 (165–340 cm).

Depth (cm)	165–170	205–210	215–220	225–230	235–240	245–250	255–260	265–270	275–280	285–290	295–300	305–310	315–320	325–330	335–340
Cyprideis torosa	19.35	48.39	55.43	71.55	19.62	15.25	24.12	4.76	11.20	10.20	18.18	0.00	0.00	0.00	0.00
A. convexa	0.00	0.00	0.00	0.00	0.00	0.00	0.00	0.00	0.00	4.08	0.00	0.00	0.00	0.00	0.00
***Aurila* spp.**	0.00	0.00	0.00	0.00	0.00	0.00	0.50	0.40	0.00	4.08	0.00	0.00	0.00	0.00	0.00
Aurila woodwardii	25.81	14.84	26.09	6.28	14.71	11.36	7.54	10.32	13.60	6.12	15.91	0.00	0.00	0.00	0.00
***Phlyctenophora* sp.**	14.52	1.61	2.72	5.02	18.53	15.84	28.14	19.84	13.60	16.33	13.64	0.00	0.00	0.00	0.00
Heterocypris salina	0.00	0.00	0.00	0.00	0.00	0.00	0.00	0.00	0.00	0.00	0.00	0.00	0.00	0.00	0.00
***Xestoleberis* communis**	0.00	1.61	0.54	1.26	5.72	9.42	6.53	5.95	0.00	8.16	11.36	0.00	0.00	0.00	0.00
***Xestoleberis* spp.**	11.29	7.74	4.89	0.00	0.00	0.00	0.00	0.00	0.00	6.12	2.27	0.00	0.00	0.00	0.00
Basslerites berchoni	0.00	0.00	0.00	0.00	1.09	1.49	0.00	1.59	0.00	0.00	0.00	0.00	0.00	0.00	0.00
Loxoconcha affinis	0.00	14.52	4.89	12.97	34.06	36.02	26.13	36.11	40.00	16.33	22.73	0.00	0.00	0.00	0.00
***Loxoconcha* sp.**	0.00	0.00	0.54	0.00	0.00	0.75	2.01	0.00	1.60	0.00	4.55	0.00	0.00	0.00	0.00
***Leptocythere* sp.**	3.23	2.90	1.09	2.51	1.91	5.23	1.01	7.14	6.40	6.12	4.55	0.00	0.00	0.00	0.00
***Urocythereis* sp.**	8.06	0.00	0.54	0.00	0.00	0.30	0.50	0.40	0.00	6.12	4.55	0.00	0.00	0.00	0.00
***Pontocythere* spp.**	1.61	0.00	0.00	0.00	0.00	0.60	0.50	1.59	1.60	4.08	0.00	0.00	0.00	0.00	0.00
***Callistocythere* sp.**	0.00	0.65	0.00	0.00	0.00	0.00	0.50	0.00	0.00	0.00	0.00	0.00	0.00	0.00	0.00
***Hiltermannicythere* sp.**	4.84	2.26	1.63	0.00	0.00	0.00	0.00	0.00	0.80	0.00	0.00	0.00	0.00	0.00	0.00
***Cytheretta* sp.**	0.00	0.00	0.00	0.00	0.54	0.30	0.00	0.00	0.80	2.04	0.00	0.00	0.00	0.00	0.00
***Cytherella* sp.**	8.06	4.84	1.09	0.00	0.27	0.45	0.50	0.00	0.00	0.00	0.00	0.00	0.00	0.00	0.00
***Eucytherura* sp.**	0.00	0.00	0.00	0.00	0.27	0.00	0.00	0.00	0.00	0.00	0.00	0.00	0.00	0.00	0.00
***Propontocypris* sp.**	0.00	0.00	0.00	0.00	0.00	0.60	1.01	7.14	0.00	0.00	0.00	0.00	0.00	0.00	0.00
***Sagmatocythere* sp.**	0.00	0.00	0.00	0.42	0.54	0.30	0.00	0.40	0.00	6.12	0.00	0.00	0.00	0.00	0.00
***Triebelina* sp.**	0.00	0.00	0.00	0.00	0.00	0.00	0.00	0.40	0.00	0.00	0.00	0.00	0.00	0.00	0.00
***Semicytherura* sp.**	0.00	0.00	0.00	0.00	2.18	1.35	0.50	2.78	8.00	2.04	2.27	0.00	0.00	0.00	0.00
not identified	3.23	0.65	0.54	0.00	0.54	0.75	0.50	1.19	2.40	2.04	0.00	0.00	0.00	0.00	0.00

Table A9. Presence-absence data of benthic foraminifera taxa recorded at the studied cores. (black dots represent the presence of data of benthic foraminifera taxa recorded at the studied cores).

Depth (cm)	Miliolidae	*A. tepida*	*A. parkinsoniana*	*A. beccarii*	*Elphidium* spp.	*Valvulineria* spp.	*Cibicides* spp.	*N. lucifuga*	*P. planatus*
AKC1									
1–5	•	•							
15–20	•	•							
30–35	•	•							
40–45	•	•							
50–55	•	•							
60–65	•	•							
70–75		•							
80–85	•	•	•						
90–95	•	•	•				•		
100–105	•	•	•		•				
110–115	•	•	•						
120–125	•	•	•		•				
130–135	•								
140–145	•	•			•	•	•	•	
145–150									
155–160									
170–175	•	•			•	•	•		
180–185	•								
190–195	•								
200–205	•	•	•		•		•	•	
210–215	•								
220–225	•				•			•	
230–235	•	•					•		
240–245	•	•	•						
250–255	•	•			•		•	•	
260–265	•								
AKC2									
5–10	•			•					•
30–35	•			•					•
35–40	•			•					•
45–50	•								•
55–60	•								
65–70	•								
75–80	•			•					
85–90	•			•					
95100									
105–110									
115–120									
125–130									
140–145									
155–160									
170–175									
180–185	•	•							•
190–195	•								•
AKC3									
5–10	•	•		•					
15–20	•			•					
25–30	•			•					
35–40									
45–50				•					
55–60				•					
65–70	•			•					
75–80				•					
85–90	•	•							
95–100	•			•					
105–110									
115–120									
125–130									
135–140									
145–150									
165–170									
205–210									
215–220									
225–230	•	•							•
235–240	•	•							
245–250	•	•							
255–260		•							
265–270		•							
275–280		•							
285–290		•							
295–300		•							
305–310									
315–320									
325–330									
335–340									

References

1. Taffs, K.H.; Saunders, K.M.; Weckström, K.; Gell, P.A.; Skilbeck, C.G. Introduction to the Application of Paleoecological Techniques in Estuaries. In *Applications of Paleoenvironmental Techniques in Estuarine Studies*; Springer: Dordrecht, The Netherlands, 2017; pp. 1–6.
2. Kjerfve, B. Comparative Oceanography of Coastal Lagoons. In *Estuarine Variability*; Academic Press: Waltham, MA, USA, 1986; pp. 63–81. [CrossRef]
3. Kjerfve, B.; Magill, K. Geographic and hydrodynamic characteristics of shallow coastal lagoons. *Mar. Geol.* **1989**, *88*, 187–199. [CrossRef]
4. Kjerfve, B. Chapter 1 Coastal Lagoons. In *Mesoscale/Synoptic Coherent Structures in Geophysical Turbulence*; Elsevier: Amsterdam, The Netherlands, 1994; Volume 60, pp. 1–8. [CrossRef]
5. Esteves, F.; Caliman, A.; Santangelo, J.; Guariento, R.D.; Farjalla, V.; Bozelli, R. Neotropical coastal lagoons: An appraisal of their biodiversity, functioning, threats and conservation management. *Braz. J. Biol.* **2008**, *68*, 967–981. [CrossRef]
6. Sacchi, M.; Molisso, F.; Pacifico, A.; Vigliotti, M.; Sabbarese, C.; Ruberti, D. Late-Holocene to recent evolution of Lake Patria, South Italy: An example of a coastal lagoon within a Mediterranean delta system. *Glob. Planet. Chang.* **2014**, *117*, 9–27. [CrossRef]
7. D'Orefice, M.; Bellotti, P.; Bertini, A.; Calderoni, G.; Neri, P.C.; Di Bella, L.; Fiorenza, D.; Foresi, L.M.; Louvari, M.A.; Rainone, L.; et al. Holocene Evolution of the Burano Paleo-Lagoon (Southern Tuscany, Italy). *Water* **2020**, *12*, 1007. [CrossRef]
8. López-Belzunce, M.; Blázquez, A.; Carmona, P.; Ruiz, J. Multi proxy analysis for reconstructing the late Holocene evolution of a Mediterranean Coastal Lagoon: Environmental variables within foraminiferal assemblages. *Catena* **2020**, *187*, 104333. [CrossRef]
9. Karkani, A.; Evelpidou, N.; Giaime, M.; Marriner, N.; Morhange, C.; Spada, G. Late Holocene sea-level evolution of Paros Island (Cyclades, Greece). *Quat. Int.* **2019**, *500*, 139–146. [CrossRef]
10. Evelpidou, N.; Pavlopoulos, K.; Vouvalidis, K.; Syrides, G.; Triantaphyllou, M.; Karkani, A.; Paraschou, T. Holocene palaeogeographical reconstruction and relative sea-level changes in the southeastern part of the island of Samos (Greece). *Comptes Rendus Geosci.* **2019**, *351*, 451–460. [CrossRef]
11. Vacchi, M.; Marriner, N.; Morhange, C.; Spada, G.; Fontana, A.; Rovere, A. Multiproxy assessment of Holocene relative sea-level changes in the western Mediterranean: Sea-level variability and improvements in the definition of the isostatic signal. *Earth Sci. Rev.* **2016**, *155*, 172–197. [CrossRef]
12. Sander, L.; Hede, M.U.; Fruergaard, M.; Nielsen, L.H.; Clemmensen, L.B.; Kroon, A.; Johannessen, P.N.; Pejrup, M. Coastal lagoons and beach ridges as complementary sedimentary archives for the reconstruction of Holocene relative sea-level changes. *Terra Nova* **2016**, *28*, 43–49. [CrossRef]
13. Stock, F.; Seyer, M.; Symanczyk, A.; Uncu, L.; Brückner, H. On the geoarchaeology of Limyra (SW Anatolia)—new insights into the famous Lycian city and its environs. *Geoarchaeology* **2020**, *35*, 487–502. [CrossRef]
14. Berndt, C.; Frenzel, P.; Çiner, A.; Ertunç, G.; Yıldırım, C. Holocene marginal marine ostracod successions from the Kızılırmak River delta; Implications for depositional environments and sea-level changes at the Southern Black Sea coast. *Sediment. Geol.* **2019**, *382*, 103–121. [CrossRef]
15. Katrantsiotis, C.; Kylander, M.E.; Smittenberg, R.; Yamoah, K.K.; Hättestrand, M.; Avramidis, P.; Strandberg, N.A.; Norström, E. Eastern Mediterranean hydroclimate reconstruction over the last 3600 years based on sedimentary n-alkanes, their carbon and hydrogen isotope composition and XRF data from the Gialova Lagoon, SW Greece. *Quat. Sci. Rev.* **2018**, *194*, 77–93. [CrossRef]
16. Horne, D.J.; Cohen, A.; Martens, K. Taxonomy, morphology and biology of Quaternary and living ostracoda. In *Large Igneous Provinces*; American Geophysical Union (AGU): Washington, DC, USA, 2002; pp. 5–36.
17. Cohen, A.C.; Peterson, D.E.; Maddocks, R.F. Ostracoda. In *The Light & Smith Manual: Intertidal Invertebrates from Central California to Oregon*; Carlton, J.T., Ed.; University of California Press: Berkeley, CA, USA, 2007; pp. 417–446.
18. Pavlopoulos, K.; Karkanas, P.; Triantaphyllou, M.; Karymbalis, E.; Tsourou, T.; Palyvos, N. Paleoenvironmental Evolution of the Coastal Plain of Marathon, Greece, during the Late Holocene: Depositional Environment, Climate, and Sea Level Changes. *J. Coast. Res.* **2006**, *222*, 424–438. [CrossRef]
19. Triantaphyllou, M.; Kouli, K.; Tsourou, T.; Koukousioura, O.; Pavlopoulos, K.; Dermitzakis, M. Paleoenvironmental changes since 3000 BC in the coastal marsh of Vravron (Attica, SE Greece). *Quat. Int.* **2010**, *216*, 14–22. [CrossRef]
20. Tsourou, T.; Drinia, H.; Anastasakis, G. Ostracod assemblages from HoloceneMiddle Shelf Deposits of southern Evoikos Gulf (Central Aegean Sea, Greece) and their palaeoenvironmental implications. *Micropaleontology* **2015**, *61*, 85–99.
21. Bernhard, J.; Reimers, C.E. Benthic foraminiferal population fluctuations related to anoxia: Santa Barbara Basin. *Biogeochem.* **1991**, *15*, 127–149. [CrossRef]
22. Corliss, B.; Silva, K.A. Rapid growth of deep-sea benthic foraminifera. *Geology* **1993**, *21*, 991–994. [CrossRef]
23. Gupta, B.K.S.; Turner, R.E.; Rabalais, N.N. Seasonal oxygen depletion in continental-shelf waters of Louisiana: Historical record of benthic foraminifers. *Geology* **1996**, *24*, 227–230. [CrossRef]
24. Drinia, H.; Antonarakou, A.; Anastasakis, G. Late Quaternary micropalaeontological record of a semi-enclosed marine basin, North Evoikos, central Aegean Sea. *Quat. Int.* **2014**, *345*, 18–31. [CrossRef]
25. Drinia, H.; Antonarakou, A.; Tsourou, T.; Kontakiotis, G.; Psychogiou, M.; Anastasakis, G. Foraminifera eco-biostratigraphy of the southern Evoikos outer shelf, central Aegean Sea, during MIS 5 to present. *Cont. Shelf Res.* **2016**, *126*, 36–49. [CrossRef]

26. Louvari, M.A.; Drinia, H.; Kontakiotis, G.; Di Bella, L.; Antonarakou, A.; Anastasakis, G. Impact of latest-glacial to Holocene sea-level oscillations on central Aegean shelf ecosystems: A benthic foraminiferal palaeoenvironmental assessment of South Evoikos Gulf, Greece. *J. Mar. Syst.* **2019**, *199*, 103181. [CrossRef]
27. Kaniewski, D.; Marriner, N.; Cheddadi, R.; Fischer, P.M.; Otto, T.; Luce, F.; Van Campo, E. Climate Change and Social Unrest: A 6000-Year Chronicle From the Eastern Mediterranean. *Geophys. Res. Lett.* **2020**, *47*, 47. [CrossRef]
28. Morhange, C.; Goiran, J.-P.; Bourcier, M.; Carbonel, P.; Le Campion, J.; Rouchy, J.-M.; Yon, M. Recent Holocene paleoenvironmental evolution and coastline changes of Kition, Larnaca, Cyprus, Mediterranean Sea. *Mar. Geol.* **2000**, *170*, 205–230. [CrossRef]
29. Vacchi, M.; Ermolli, E.R.; Morhange, C.; Ruello, M.R.; Di Donato, V.; Di Vito, M.A.; Giampaola, D.; Carsana, V.; Liuzza, V.; Cinque, A.; et al. Millennial variability of rates of sea-level rise in the ancient harbour of Naples (Italy, western Mediterranean Sea). *Quat. Res.* **2019**, *93*, 284–298. [CrossRef]
30. Lambeck, K.; Antonioli, F.; Anzidei, M.; Ferranti, L.; Leoni, G.; Scicchitano, G.; Silenzi, S. Sea level change along the Italian coast during the Holocene and projections for the future. *Quat. Int.* **2011**, *232*, 250–257. [CrossRef]
31. Wahl, T.; Haigh, I.D.; Nicholls, R.J.; Arns, A.; Dangendorf, S.; Hinkel, J.; Slangen, A.B.A. Understanding extreme sea levels for broad-scale coastal impact and adaptation analysis. *Nat. Commun.* **2017**, *8*, 16075. [CrossRef]
32. Antonioli, F.; Anzidei, M.; Amorosi, A.; Presti, V.L.; Mastronuzzi, G.; Deiana, G.; De Falco, G.; Fontana, A.; Fontolan, G.; Lisco, S.; et al. Sea-level rise and potential drowning of the Italian coastal plains: Flooding risk scenarios for 2100. *Quat. Sci. Rev.* **2017**, *158*, 29–43. [CrossRef]
33. Bear, L.; Morel, S. *The Geology and Mineral Resources of the Agros-Akrotiri Area*; Geological Survey Department: Lefkosia, Cyprus, 1960.
34. Polidorou, M.; Saitis, G.; Evelpidou, N. Beachrock development as an indicator of paleogeographic evolution, the case of Akrotiri Peninsula, Cyprus. *Zeitschrift für Geomorphologie* **2021**, *63*, 3–17. [CrossRef]
35. Eaton, S.; Robertson, A. The Miocene Pakhna Formation, southern Cyprus and its relationship to the Neogene tectonic evolution of the Eastern Mediterranean. *Sediment. Geol.* **1993**, *86*, 273–296. [CrossRef]
36. Soulas, J.P. *Active Tectonics Studies in Cyprus for Seismic Risk Mitigation: The Greater Limassol Area*; Cyprus Geological Survey: Nicosia, Cyprus, 1999.
37. Simmons, A.H. Humans, island colonization and Pleistocene extinctions in the Mediterranean: The view from Akrotiri Aetokremnos, Cyprus. *Antiquity* **1991**, *65*, 857–869. [CrossRef]
38. Mandel, R.D.; Simmons, A.H. Geoarchaeology of the AkrotiriAetokremnos rockshelter, Southern Cyprus. *Geoarchaeology* **1997**, *12*, 567–605. [CrossRef]
39. Wigand, P.; Simmons, A.H. The Dating of Akortiri Aetokremnos. In *Perspectives on the Archaeology of Pipes, Tobacco and Other Smoke Plants in the Ancient Americas*; Springer: Boston, MA, USA, 2002; pp. 193–215. [CrossRef]
40. Ammerman, A.J.; Noller, J.S. New light on Aetokremnos. *World Archaeol.* **2005**, *37*, 533–543. [CrossRef]
41. Simmons, A.; Mandel, R. Not such a new light: A response to Ammerman and Noller. *World Archaeol.* **2007**, *39*, 475–482. [CrossRef]
42. James, S. Excavations of Roman/Early Byzantine Structures at Dreamers Bay, Akrotiri. *Bull. Counc. Br. Res. Levant* **2017**, *12*, 44–47. [CrossRef]
43. James, S.; Score, V. Akrotiri-Dreamer's Bay (Nissarouin) Excavation & Survey. In *Spring 2018 Interim Report*; Honor Frost Foundation: London, UK, 2018.
44. Blue, L. Ancient Akrotiri Project, Dreamer's Bay Underwater Survey. In *Interim Report 2018*; Honor Frost Foundation: London, UK, 2018.
45. Folk, R.L. The Distinction between Grain Size and Mineral Composition in Sedimentary-Rock Nomenclature. *J. Geol.* **1954**, *62*, 344–359. [CrossRef]
46. Rothwell, R.G.; Croudace, I.W. Micro-XRF Studies of Sediment Cores: A Perspective on Capability and Application in the Environmental Sciences. In *Applications of Paleoenvironmental Techniques in Estuarine Studies*; Springer: Dordrecht, The Netherlands, 2015; pp. 1–21. [CrossRef]
47. Haenssler, E.; Unkel, I.; Dörfler, W.; Nadeau, M.-J. Driving mechanisms of Holocene lagoon development and barrier accretion in Northern Elis, Peloponnese, inferred from the sedimentary record of the Kotychi Lagoon. *E G Quat. Sci. J.* **2014**, *63*, 60–77. [CrossRef]
48. Emmanouilidis, A.; Katrantsiotis, C.; Norström, E.; Risberg, J.; Kylander, M.; Sheik, T.A.; Iliopoulos, G.; Avramidis, P. Middle to late Holocene palaeoenvironmental study of Gialova Lagoon, SW Peloponnese, Greece. *Quat. Int.* **2018**, *476*, 46–62. [CrossRef]
49. Brunović, D.; Miko, S.; Hasan, O.; Papatheodorou, G.; Ilijanić, N.; Miserocchi, S.; Correggiari, A.; Geraga, M. Late Pleistocene and Holocene paleoenvironmental reconstruction of a drowned karst isolation basin (Lošinj Channel, NE Adriatic Sea). *Palaeogeogr. Palaeoclim. Palaeoecol.* **2020**, *544*, 109587. [CrossRef]
50. Rothwell, R.G.; Hoogakker, B.; Thomson, J.; Croudace, I.; Frenz, M. Turbidite emplacement on the southern Balearic Abyssal Plain (western Mediterranean Sea) during Marine Isotope Stages 1–3: An application of ITRAX XRF scanning of sediment cores to lithostratigraphic analysis. *Geol. Soc. Spec. Publ.* **2006**, *267*, 79–98. [CrossRef]
51. Yarincik, K.M.; Murray, R.W.; Peterson, L.C. Climatically sensitive eolian and hemipelagic deposition in the Cariaco Basin, Venezuela, over the past 578,000 years: Results from Al/Ti and K/Al. *Paleoceanography* **2000**, *15*, 210–228. [CrossRef]

52. Calvert, S.; Pedersen, T. Chapter Fourteen Elemental Proxies for Palaeoclimatic and Palaeoceanographic Variability in Marine Sediments: Interpretation and Application. In *Earth and Life Processes Discovered from Subseafloor Environments—A Decade of Science Achieved by the Integrated Ocean Drilling Program (IODP)*; Elsevier: Amsterdam, The Netherlands, 2007; pp. 567–644. [CrossRef]
53. Bahr, A.; Lamy, F.; Arz, H.W.; Major, C.; Kwiecien, O.; Wefer, G. Abrupt changes of temperature and water chemistry in the late Pleistocene and early Holocene Black Sea. *Geochem. Geophys. Geosyst.* **2008**, *9*. [CrossRef]
54. Van Hoang, L.; Clift, P.D.; Schwab, A.M.; Huuse, M.; Nguyen, D.A.; Zhen, S. Large-scale erosional response of SE Asia to monsoon evolution reconstructed from sedimentary records of the Song Hong-Yinggehai and Qiongdongnan basins, South China Sea. *Geol. Soc. Spec. Publ.* **2010**, *342*, 219–244. [CrossRef]
55. Tjallingii, R.; Stattegger, K.; Wetzel, A.; Van Phach, P. Infilling and flooding of the Mekong River incised valley during deglacial sea-level rise. *Quat. Sci. Rev.* **2010**, *29*, 1432–1444. [CrossRef]
56. Barbeito-Gonzalez, P.J. Die Ostracoden des Küstenbereiches von Naxos (Griechenland) und ihre Lebensbereiche. *Mitt. Aus. Dem. Hambg. Zool. Mus. Und Inst.* **1971**, *67*, 255–326.
57. Bonaduce, G.; Ciampo, G.; Masoli, M. Distribution of Ostracods in the Adriatic Sea. *Pubbl. Staz. Zool. Napoli* **1975**, *40*, 1–304.
58. Athersuch, J. The ecology and distribution of the littoral ostracods of Cyprus. *J. Nat. Hist.* **1979**, *13*, 135–160. [CrossRef]
59. Stambolidis, E. Subrezente Ostracoden aus dem Evros-Delta (Griechenland) Einschliesslich der Entwicklung des Schlosses Gewisser Arten. Ph.D. Thesis, Acta Universitatis Upsaliensis, Uppsala, Sweden, 1984.
60. Athersuch, J.; Horne, D.J.; Whittaker, J.E. *Marine and brackish water ostracods (superfamilies Cypridacea and Cytheracea). Synopses of the British Fauna (New Series)*; Ghent University Library: Ghent, Belgium, 1989; Volume 43, p. 343.
61. Barbieri, G.; Vaiani, S.C. Benthic foraminifera or Ostracoda? Comparing the accuracy of palaeoenvironmental indicators from a Pleistocene lagoon of the Romagna coastal plain (Italy). *J. Micropalaeontol.* **2018**, *37*, 203–230. [CrossRef]
62. Cimerman, F.; Langer, M.R. Mediterranean Foraminifera. *Acad. Sci. Artium Slov. Ljubl.* **1991**, *30*, 1–11.
63. Jorissen, F.J. *Benthic Foraminiferal Microhabitats below the Sediment-Water Interface*; Springer Science and Business Media LLC: Larkspur, CA, USA, 1999; pp. 161–179. [CrossRef]
64. Sgarrella, F.; DI Donato, V.; Sprovieri, R. Benthic foraminiferal assemblage turnover during intensification of the Northern Hemisphere glaciation in the Piacenzian Punta Piccola section (Southern Italy). *Palaeogeogr. Palaeoclim. Palaeoecol.* **2012**, *333–334*, 59–74. [CrossRef]
65. Moissette, P.; Koskeridou, E.; Drinia, H.; Cornée, J.-J. Facies associations in warm-temperate siliciclastic deposits: Insights from early Pleistocene eastern Mediterranean (Rhodes, Greece). *Geol. Mag.* **2016**, *153*, 61–83. [CrossRef]
66. Stuiver, M.; Reimer, P.; Sept, R.R.-W. CALIB Radiocarbon Calibration. Available online: http://calib.org/calib/ (accessed on 20 April 2021).
67. Reimer, P.J.; Bard, E.; Bayliss, A.; Beck, J.W.; Blackwell, P.G.; Ramsey, C.B.; Buck, C.; Cheng, H.; Edwards, R.L.; Friedrich, M.; et al. IntCal13 and Marine13 Radiocarbon Age Calibration Curves 0–50,000 Years cal BP. *Radiocarbon* **2013**, *55*, 1869–1887. [CrossRef]
68. Reimer, P.J.; McCormac, F.G. Marine Radiocarbon Reservoir Corrections for the Mediterranean and Aegean Seas. *Radiocarbon* **2002**, *44*, 159–166. [CrossRef]
69. Blott, S.J.; Pye, K. Gradistat: A grain size distribution and statistics package for the analysis of unconsolidated sediments. *Earth Surf. Process. Landf.* **2001**, *26*, 1237–1248. [CrossRef]
70. Van Morkhoven, F.P.C.M. *Post-Palaeozoic Ostracoda: Their Morphology, Taxonomy and Economic Use*; Elsevier: Amsterdam, The Netherlands, 1962; Volume 1.
71. Meisch, C. Freshwater Ostracoda of Western and Central Europe. In *Süßwasserfauna von Mitteleuropa*; Schwoerbel, J., Zwick, P., Eds.; Spektrum Akademischer Verlag: Berlin/Heidelberg, Germany, 2000; p. 522.
72. Salel, T.; Bruneton, H.; Lefèvre, D. Ostracods and environmental variability in lagoons and deltas along the north-western Mediterranean coast (Gulf of Lions, France and Ebro delta, Spain). *Revue Micropaléontologie* **2016**, *59*, 425–444. [CrossRef]
73. Carboni, M.G.; Bergamin, L.; Di Bella, L.; Iamundo, F.; Pugliese, N. Palaeoecological evidences from foraminifers and ostracods on Late Quaternary sea-level changes in the Ombrone river plain (central Tyrrhenian coast, Italy). *Geobios* **2002**, *35*, 40–50. [CrossRef]
74. Cabral, M.; Freitas, M.; Andrade, C.; Cruces, A. Coastal evolution and Holocene ostracods in Melides lagoon (SW Portugal). *Mar. Micropaleontol.* **2006**, *60*, 181–204. [CrossRef]
75. Tsourou, T. Composition and Distribution of Recent Marine Ostracod Assemblages in the Bottom Sediments of Central Aegean Sea (SE Andros Island, Greece). *Int. Rev. Hydrobiol.* **2012**, *97*, 276–300. [CrossRef]
76. Leroy, S.; Kazancı, N.; Ileri, Ö.; Kibar, M.; Emre, Ö.; McGee, E.; Griffiths, H. Abrupt environmental changes within a late Holocene lacustrine sequence south of the Marmara Sea (Lake Manyas, N-W Turkey): Possible links with seismic events. *Mar. Geol.* **2002**, *190*, 531–552. [CrossRef]
77. Croudace, I.; Rindby, A.; Rothwell, R.G. ITRAX: Description and evaluation of a new multi-function X-ray core scanner. *Geol. Soc. Spec. Publ.* **2006**, *267*, 51–63. [CrossRef]
78. Goudeau, M.L.; Grauel, A.-L.; Tessarolo, C.; Leider, A.; Chen, L.; Bernasconi, S.; Versteegh, G.J.; Zonneveld, K.A.; Boer, W.; Alonso-Hernandez, C.; et al. The Glacial–Interglacial transition and Holocene environmental changes in sediments from the Gulf of Taranto, central Mediterranean. *Mar. Geol.* **2014**, *348*, 88–102. [CrossRef]
79. Jorissen, F. Benthic foraminifera from the Adriatic Sea: Principles of phenotypic variation. Ph.D. Thesis, Utrecht University, Utrecht, The Netherlands, 1988.

80. Murray, J.W. Ecology and Applications of Benthic Foraminifera. In *Ecology and Applications of Benthic Foraminifera*; Cambridge University Press: Cambridge, UK, 2006.
81. Bustron, F. *Chronique de L'île de Chypre*; Ministre de l'Instruction Publique et des Beaux Arts: Paris, France, 1886.